CONSTRUCTION OF WEIGHTED UPWIND COMPACT SCHEME

by

ZHENGJIE WANG

Presented to the Faculty of the Graduate School of
The University of Texas at Arlington in Partial Fulfillment
of the Requirements
for the Degree of

DOCTOR OF PHILOSOPHY

THE UNIVERSITY OF TEXAS AT ARLINGTON
MAY 2015

Acknowledgements

I would like to thank my research advisor and Committee Chairman, Dr. Chaoqun Liu. Without Dr. Liu's elaborate guide, inexhaustible inspiration, and tenacious patience, I would not have the perseverance to change myself from numerically ignorance to having some computation sense, also very fortunately having several academic publications. It is my most significant honor to work, to learn with Dr. Liu.

I would also like to appreciate committee members Dr. Benito Chen-Charpentier, Dr. Guojun Liao, Dr. Hristo Kojouharov, Dr. Jianzhong Su and Dr. Ren-cang Li for their understanding and support.

I must express my gratitude to the Department of Mathematics, for the financial support through Graduate Teaching Assistantships, and I would also like to appreciate all colleagues for making my time at the University of Texas at Arlington a great experience. Meanwhile, I appreciate Götaverken Arendal (GVA) significantly. Without GVA's understanding and support, I would not be able to finish the dissertation in Houston.

Finally, I appreciate my families for coming along with me all these years.

April 20, 2015

Abstract

CONSTRUCTION OF WEIGHTED

UPWIND COMPACT SCHEME

Zhengjie Wang, PhD

The University of Texas at Arlington, 2015

Supervising Professor: Chaoqun Liu

Enormous endeavor has been devoted in spatial high order high resolution schemes in more than twenty five years previously, like total variation diminishing (TVD), essentially non-oscillatory scheme, weighted essentially non-oscillatory scheme for finite difference, and Discontinuous Galerkin methods for finite element and the finite volume.

In this dissertation, a high order finite difference Weighted Upwind Compact Scheme has been constructed by dissipation and dispersion analysis. Secondly, a new method to construct global weights has been tested. Thirdly, a methodology to compromise dissipation and dispersion in constructing Weighted Upwind Compact Scheme has been derived. Finally, several numerical test cases have been shown.

Table of Contents

List of Illustrations

List of Tables

Chapter 1

Introduction

Along with computer's hardware capabilities and parallel algorithm developing, extensively applying numerical scheme is becoming a more appreciable trend. Nowadays, not only Computational Fluid Dynamics but also more and more other fields such as Computational Aero-acoustics [1], Seismic Imaging [2], Reservoir Engineering, Financial Engineering [3], Image Processing, and so on are relying on high order numerical schemes to obtain high accuracy derivatives. The developments in Computational Fluid Dynamics include mesh generation improvements, solver efficiency enhancement, parallel algorithm efficiency enhancement, and visualization improvements. Especially, the applications of CFD has been more extensive, more complicated, and more applicable to realities' problem than ever before, such as aerodynamics, hydrodynamics, meteorology, ship engineering, offshore engineering, subsea engineering, water, chemical engineering, construction, machinery, automobile industry, ocean engineering, sports, environmental engineering, medical and health.

Also in Computational Fluid Dynamics, there have been more and more challenges emerging with all application profits. Simulation of complex flow is one of the challenges. The complex flow can be caused by complex geometry, flow instability, high temperature, multi-phase, and unsteady multi-scale flow structure. In this dissertation, multi-scale complex flow with shock is the major application field of a newly studied higher order numerical scheme.

Numerical scheme is the numerical method of calculating approximations of derivatives of a given data. Lewis Fry Richardson, an English Mathematician, who is also a meteorologist, used central difference scheme for numerical weather forecasting in 1910 [4]. This is considered as the idea of CFD origin [5]. Later, three German

mathematicians, Richard Courant, Kurt Otto Friedrichs and Hans Lewy analyzed the stability of numerical scheme in 1928 [6]. Very famous and widely used CFL stability condition for numerical computation is based on their analysis work [7]. John Von Neumann and R. D. Richtmyer introduced additional artificial viscosity term in the equation of hydrodynamics to capture shocks [8]. A first-order accurate upwind finite difference scheme was developed for solving the nonlinear hyperbolic equations by Courant, Isaacson and Rees in 1952 [9]. Their method was based on the normal or characteristic form of the quasi-linear first order hyperbolic system. With the idea in mind of preserving the domain of dependence, the spatial derivative in each direction of the characteristic form was approximated by either a first-order forward or backward finite difference quotient depending upon whether the local eigenvalue (characteristic speed) is negative or positive [10]. The notion of eigenvalue splitting was introduced to provide the automatic switching for constructing uniform upwind finite difference schemes. Lax [11] and Friedirchs [12] developed a first order central finite difference scheme for linear convection equations [13]. After that, scientists developed a lot of first order scheme. Until 1959, Godunov published an upwind scheme with his name, which gave a new path for constructing CFD scheme [14]. This new path is through numerical approximation of Riemann Problem's solution, which is still important to todays' CFD research.

From Lax milestone work [15] in 1957, more and more scientists like Wendroff, Richtmyer and Morton enriched numerical scheme. The Lax-Wendroff scheme [16] is like the prototype of modern CFD, and the development from Lax-Wendroff scheme became the cornerstone of modern CFD [17]. The Lax–Wendroff scheme, named after Peter Lax and Burton Wendroff, is a numerical scheme for the solution of hyperbolic partial differential equations, based on finite differences. It is second-order accurate in both space and time. This method is an example of explicit time integration where the function

that defines governing equation is evaluated at the current time. The most famous development of Lax-Wendroff scheme is MacCormack method [18, 19], which is simpler than Lax-Wendroff scheme. This two-step second-order finite difference method was introduced by Robert W. MacCormack in 1969. The MacCormack method is elegant and easy to understand and program. MacCormack method became the leading role of two-dimensional steady flow simulation in last century's 70s. But these second-order schemes might have non-physics oscillation around discontinuities, like pressure and density numerical oscillation around shock wave. This short-coming limited the application of these second-order schemes in shock problems [17].

Bram van Leer created MUSCL (monotone upstream-centered schemes for conservation laws) method in 1979 [20]. The MUSCL scheme is a finite volume method that can provide highly accurate numerical solutions for a given system, even in cases where the solutions exhibit shocks, discontinuities, or large gradients. The MUSCL used the idea that replacing the piecewise constant approximation of Godunov's scheme by reconstructed states, derived from cell-averaged states obtained from the previous time-step. For each cell, slope limited, reconstructed left and right states are obtained and used to calculate fluxes at the cell boundaries (edges). These fluxes can, in turn, be used as input to a Riemann solver, following which the solutions are averaged and used to advance the solution in time [21].

Ami Harten brought up total variation non-increasing and monotonicity preserving concepts for finite-difference scheme in 1983 [22]. Ami Harten started TVD (total variation diminishing) scheme which is a second order scheme with high resolution and can damp non-physics oscillation around shock. Following Ami Harten, many scientists created many different kinds of TVD schemes, since TVD scheme has properties of high resolution and shock-capturing with non-oscillation properties. Ami Harten, Bjorn

Engquist, Stanley Osher, and Sukumar R. Chakravarthy continued the construction and analysis of essentially non-oscillartory shock capturing methods for the approximation of hyperbolic conservation laws, and proposed uniformly high order accurate essentially non-oscillatory schemes which keeps high order accuracy around shocks [23]. Xu-Dong Liu, Stanley Osher, and Tony Chan introduced a new version of ENO (essentially non-oscillatory) shock-capturing schemes which called weighted ENO [24]. The main idea is that, instead of choosing the “smoothest” stencil to pick one interpolating polynomial for the ENO reconstruction, using a convex combination of all candidates’ stencils to achieve the essentially non-oscillatory property, while additionally obtaining one order of improvement in accuracy. The resulting WENO (weighted ENO) schemes are based on cell averages and a TVD Runge-Kutta time discretization [17].

Sanjiva K. Lele deeply and thoroughly studied compact finite difference scheme by Fourier analysis of dissipation and dispersion [25]. This analysis testified that compact scheme has high order accuracy and high resolution. Then compact scheme has been widely applied in Direct Numerical Analysis, Large Eddy Simulation and Computational Acoustics. But directly using compact scheme to solve flow with shocks will cause non-physical oscillation. Many efforts have been devoted into giving artificial dissipation for compact scheme to damping non-physical oscillations. Some other efforts were combine and switch compact scheme with ENO/WENO. This combination and switch method will create spurious oscillation around switch point, and this oscillation will contaminate smooth area solution finally [17]. The Fourier analysis dissipation and dispersion is the base tool for studying Weighted Upwind Compact Scheme in this dissertation.

Central finite difference scheme needs artificial viscosity terms to give high frequency damping to restrain non-physics oscillation around shocks and stagnation points. Even though, the artificial viscosity terms have two issues. First, calculating

artificial viscosity increased computation hours; second, the high frequency damping from artificial viscosity term might not be adaptive for all kinds of problems [17].

The construction of upwind scheme represents fluid mechanics equations' fundamental physics properties, like propagation direction of wave, flux. For representing different physics properties, different upwind schemes have been constructed. So far, there are two ways for upwind scheme to present physics properties. The first way is by using eigenvalue's sign to construct upwind scheme. This kind upwind scheme's flux splitting and directional discretization are based on propagation velocity's sign; backward difference for positive propagation velocity; forward difference for negative propagation velocity. The second way is by calculating a sequence of local Riemann problems' solution, or approximating a sequence of local Riemann problem's solution. The first way of flux splitting is used for Weighted Upwind Compact Scheme in this dissertation.

Computational Fluid Dynamics is developing rapidly, and has very wide variety of numerical schemes. Traditionally, numerical schemes can be categorized into three groups by spatial discretization method. One is based on interpolation; second is flux computation; third is mixture of interpolation and flux computation, like TVD scheme.

It is crucial for a numerical scheme to find derivative value as accurate as possible with limited available computational resources, especially when dealing discontinuities with small scale problems. In Computational Fluid Dynamics, shock wave interacting with turbulent flow is this kind of sensitive and difficult problem. Reproducing turbulence structure as much as possible will require the numerical scheme only having small quantity dissipation. Otherwise, small length turbulence detail would be smeared. High order scheme would be an optimistic option for small scale problems, since high order scheme has high resolution to present small scale details. On the other hand,

capturing shock might cause non-physical oscillation for non-dissipation or very low dissipation high order scheme.

In this dissertation, an effort is spent in study a methodology of constructing weighted upwind compact scheme. The target scheme of this construction need avoid negative dissipation in left stencil for shock-capturing stability; also need utilize non-oscillatory weights to choose the best stencil or to pick up the optimized share from each stencil. Also as part of this target scheme of this construction, need an optimized dispersion in left stencil for shock-capturing stability. Another effort is spend in study a new method of creating global weights for this weighted upwind compact scheme.

The structure of this dissertation is, Chapter 2, Construction Methodology of WUCS; Chapter 3, Order, Dissipation and Dispersion Analysis; Chapter 4, 1D and 2D cases for WUCS; Chapter 5, New Method of Creating Global Weights for WUCS, Chapter 6 Construction Methodology Application, and Chapter 7 includes conclusion and discussion of WUCS.

Chapter 2

Construction Methodology of WUCS

This Chapter will start with scalar conservation equation as basic understanding of finite difference scheme, then seventh-order parametric weighted upwind compact scheme and eighth-order weighted central compact scheme will be introduced. Fourier analysis will be introduced as forging tool for constructing Weighted Upwind Compact Scheme. Finally WUCS will be forged by seventh-order parametric weighted upwind compact scheme and eighth-order weighted central compact scheme.

2.1 Numerical Formulation

The scalar conservation equation may be an example to start the study framework of finite difference numerical scheme.

$$q_t(x,t) + F_x\big(q(x,t)\big) = 0 \tag{2.1}$$

Discretizing the domain, grid points (cell interface) are defined as

$$a = x_{\frac{1}{2}} < x_{\frac{3}{2}} < \cdots < x_{N-\frac{1}{2}} < x_{N+\frac{1}{2}} = b \tag{2.2}$$

The cell centers and cell sizes are defined, respectively, as

$$x_j \equiv \frac{1}{2}\left(x_{j-\frac{1}{2}} + x_{j+\frac{1}{2}}\right) \qquad h_j \equiv x_{j+\frac{1}{2}} - x_{j-\frac{1}{2}} \qquad j = 1,2,\dots,N$$

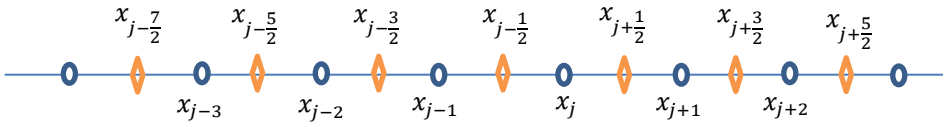

Figure 2-1 Grid for one-dimensional case

A semi-discrete conservative form of (2.1) reads as

$$\frac{dq_j}{dt} = -(\hat{F}_{j+\frac{1}{2}} - \hat{F}_{j-\frac{1}{2}})/h_j \tag{2.3}$$

where $\hat{F}$ is the numerical flux associated to the original function F, defined implicitly by $F_j = F(q(x_j, t)) \equiv \int_{x_{j-\frac{1}{2}}}^{x_{j+\frac{1}{2}}} \hat{F}(\xi) d\xi / h_j$. With the given implicit definition of the numerical flux $\hat{F}$, Eq. (2.3) constitutes as an *exact* expression of Eq. (2.1).

We denote H the primitive function of $\hat{F}(\xi)$, which can be calculated by

$$H_{j+\frac{1}{2}} = H\left(x_{j+\frac{1}{2}}\right) = \int_{-\infty}^{x_{j+\frac{1}{2}}} \hat{F}(\xi) d\xi = \sum_{i=-\infty}^{j} \int_{x_{i-\frac{1}{2}}}^{x_{i+\frac{1}{2}}} \hat{F}(\xi) d\xi = \sum_{i=-\infty}^{j} F_i \, h_i \tag{2.4}$$

So the primitive function H is calculated from the discrete data set of the original function F. The derivative of the primitive function at the cell interfaces coincides with the numerical flux, i.e.

$$H'_{j+\frac{1}{2}} = \hat{F}_{j+\frac{1}{2}}$$

From the above definitions, it is clear that

$$F'(x_j) = F'_j = (\hat{F}_{j+\frac{1}{2}} - \hat{F}_{j-\frac{1}{2}})/h_j = (H'_{j+\frac{1}{2}} - H'_{j-\frac{1}{2}})/h_j \tag{2.5}$$

In the described procedure $F \to H \to \hat{F} \to F'$, introduced by [31], the only approximation involved is the calculation of the derivative of the primitive function H', whereas all other calculations are exact.

2.2 Fifth-Order Weighted Essentially Non-Oscillatory Scheme

This section is taking 5th Order WENO as an initial example for expanding and forging compact scheme, upwind scheme, and weighted scheme in later section. The basic idea of the WENO scheme is to obtain a high-order approximation to the numerical flux by a weighted average (convex combination) of multiple lower-order candidate approximations, according to the “smoothness” of the original function on each of the candidates [27]. For obtaining a 5th order WENO, three second-order approximations of

the numerical fluxes at $\hat{F}_{j-\frac{1}{2}}$and $\hat{F}_{j+\frac{1}{2}}$ are obtained from the three candidate stencils (Figure 2-1):

$$E^0_{WENO} = \{F_{j-2}, F_{j-1}, F_j\}$$

$$E^1_{WENO} = \{F_{j-1}, F_j, F_{j+1}\}$$

$$E^2_{WENO} = \{F_j, F_{j+1}, F_{j+2}\}$$

Choosing the Lagrange polynomial for the third order approximation of $\hat{F}_{j+\frac{1}{2}}$, we obtain, for the first stencil E^0_{WENO}:

$$\hat{F}^{E^0_{WENO}}_{j+\frac{1}{2}} \approx \frac{1}{3}F_{j-2} - \frac{7}{6}F_{j-1} + \frac{11}{6}F_j$$

And similarly for the other two stencils $E^1_{WENO}$and E^2_{WENO}:

$$\hat{F}^{E^1_{WENO}}_{j+\frac{1}{2}} \approx -\frac{1}{6}F_{j-1} + \frac{5}{6}F_j + \frac{1}{3}F_{j+1}$$

$$\hat{F}^{E^2_{WENO}}_{j+\frac{1}{2}} \approx \frac{1}{3}F_j + \frac{5}{6}F_{j+1} - \frac{1}{6}F_{j+2}$$

If we take the weighted average of the three low-order approximations above, with the constant optimal weights [24] as below

$$C^0_{WENO} = \frac{1}{10} \qquad C^1_{WENO} = \frac{6}{10} \qquad C^2_{WENO} = \frac{3}{10} \tag{2.6}$$

we obtain

$$\hat{F}_{j+\frac{1}{2}} \approx \sum_{i=0}^{2} C^i_{WENO} \hat{F}^{E^i_{WENO}}_{j+\frac{1}{2}}$$

$$= \frac{1}{30}F_{j-2} - \frac{13}{60}F_{j-1} + \frac{47}{60}F_j + \frac{9}{20}F_{j+1} - \frac{1}{20}F_{j+2}$$

Note that the constant weights in (2.6) sum up to 1 for consistency, i.e. $\sum_{i=0}^{2} C^i_{WENO} = 1$. After the expression of the approximation for $\hat{F}_{j-\frac{1}{2}} = \hat{F}_{\left(j+\frac{1}{2}\right)-1}$ is obtained in analogous fashion as above, we can calculate the discrete approximation to the derivative of the original function F as (see the semi-discrete equation (2.3))

$$F'_j = (\hat{F}_{j+\frac{1}{2}} - \hat{F}_{j-\frac{1}{2}})/h_j \approx (-\frac{1}{30}F_{j-3} + \frac{1}{4}F_{j-2} - F_{j-1} + \frac{1}{3}F_j + \frac{1}{2}F_{j+1} - \frac{1}{20}F_{j+2})/h_j \qquad (2.7)$$

It is easy to verify by a Taylor series expansion that Eq. (2.7) is a 5th order approximation to the discrete derivative F'_j [26].

Instead of using the constant weights (2.6), the WENO scheme adaptively selects the weights in relation to the "smoothness" of the stencils. The non-linear weights $\omega_{WENO}^{i,j\pm\frac{1}{2}}$ are introduced as

$$\omega_{WENO}^{i,j\pm\frac{1}{2}} = \frac{\gamma_{WENO}^{i,j\pm\frac{1}{2}}}{\sum_{k=0}^{2}\gamma_{WENO}^{k,j\pm\frac{1}{2}}} \qquad \gamma_{WENO}^{i,j\pm\frac{1}{2}} = \frac{C_{WENO}^{i}}{(\varepsilon + IS_{i,j\pm\frac{1}{2}})^p} \qquad i = 0,1,2 \qquad (2.8)$$

Where ε is a small parameter which prevents the division by zero, p is an integer (set equal to 2 in [27]), C_{WENO}^{i} are those given in (2.6), and $IS_{i,j\pm\frac{1}{2}}$ are the "smoothness" indicators given in [27]. In general, $IS_{k,j-\frac{1}{2}} \neq IS_{k,j+\frac{1}{2}}$ with $k = 0,1,2$, implying that also $\omega_{WENO}^{k,j-\frac{1}{2}} \neq \omega_{WENO}^{k,j+\frac{1}{2}}$ with $k = 0,1,2$. Note that the non-linear weights need to satisfy $\sum_{k=0}^{2}\omega_{WENO}^{k,j\pm\frac{1}{2}} = 1$ for consistency of the scheme.

2.3 Seventh-Order Parametric Weighted Upwind Compact Scheme

Similar as 5th Order WENO, the intuitive drive of a Parametric Weighted Upwind Compact Scheme is to obtain seventh order approximation to the numerical flux by a weighted average of multiple lower-order compact candidate approximations, according to the "smoothness" of the original function on each of the candidates. For obtaining a 7th order Parametric Weighted Upwind Compact Scheme, three third-order approximations

of the linear compact combination of numerical fluxes at $\hat{F}_{j-\frac{3}{2}}$, $\hat{F}_{j-\frac{1}{2}}$, $\hat{F}_{j+\frac{1}{2}}$, $\hat{F}_{j+\frac{3}{2}}$and $\hat{F}_{j+\frac{5}{2}}$ are obtained from the three candidate stencils (Figure 2-1):

$$E^0 = \{F_{j-2}, F_{j-1}, F_j\}$$

$$E^1 = \{F_{j-1}, F_j, F_{j+1}\}$$

$$E^2 = \{F_j, F_{j+1}, F_{j+2}\}$$

Choosing the Lagrange polynomial for the third order approximation of $t_0\hat{F}_{j-\frac{3}{2}} + t_1\hat{F}_{j-\frac{1}{2}} + \hat{F}_{j+\frac{1}{2}}$, we obtain, for the first stencil E^0:

$$t_0\hat{F}_{j-\frac{3}{2}} + t_1\hat{F}_{j-\frac{1}{2}} + \hat{F}_{j+\frac{1}{2}} \approx (t_2F_{j-2} + t_3F_{j-1} + t_4F_j)/h \tag{2.9}$$

$$t_2 = (2 + 2t_0 - t_1)/6$$

$$t_3 = (-7 + 5t_0 + 5t_1)/6$$

$$t_4 = (11 - t_0 + 2t_1)/6$$

And similarly for the other two stencils E^1 and E^2:

$$s_0\hat{F}_{j-\frac{1}{2}} + \hat{F}_{j+\frac{1}{2}} + s_1\hat{F}_{j+\frac{3}{2}} \approx (s_2F_{j-1} + s_3F_j + s_4F_{j+1})/h \tag{2.10}$$

$$s_2 = (-1 + 2s_0 + 2s_1)/6$$

$$s_3 = (5 + 5s_0 - 7s_1)/6$$

$$s_4 = (2 - s_0 + 11s_1)/6$$

$$\hat{F}_{j+\frac{1}{2}} + r_0\hat{F}_{j+\frac{3}{2}} + r_1\hat{F}_{j+\frac{5}{2}} \approx (r_2F_j + r_3F_{j+1} + r_4F_{j+2})/h \tag{2.11}$$

$$r_2 = (2 - r_0 + 2r_1)/6$$

$$r_3 = (5 + 5r_0 - 7r_1)/6$$

$$r_4 = (-1 + 2r_0 + 11r_1)/6$$

For obtaining 7th order of $C^0E^0 + C^1E^1 + C^2E^2$, t_0, t_1, s_0, s_1, r_0, r_1, C^0, C^1, and C^2 need satisfy

$$t_0 = \frac{C^0 + C^1 + 11C^2 - 20C^2 r_0 + 107C^2 r_1}{3C^0}$$

$$t_1 = \frac{61}{24} + \frac{13C^1}{24C^0} + \frac{137C^2}{24C^0} - \frac{31C^2 \mathrm{r}_0}{3C^0}$$

$$s_0 = -\frac{25C^0 - 23C^1 - 139C^2 + 232C^2 r_0 - 1132C^2 r_1}{24C^1} \qquad (2.12)$$

$$s_1 = \frac{C^0 + C^1 - 19C^2 + 28C^2 r_0 - 124C^2 r_1}{12C^1}$$

Like WENO, this 7th order parametric weighted upwind compact scheme will use non-linear weights ω^i instead C^i

$$\omega^{i,j\pm\frac{1}{2}} = \frac{\gamma^{i,j\pm\frac{1}{2}}}{\sum_{k=0}^{2} \gamma^{k,j\pm\frac{1}{2}}} \qquad \gamma^{i,j\pm\frac{1}{2}} = \frac{C^i}{(\varepsilon + IS_{i,j\pm\frac{1}{2}})^p} \qquad i = 0,1,2 \qquad (2.13)$$

And $\omega^0 E^0 + \omega^1 E^1 + \omega^2 E^2$ is defined as 7th parametric weighted upwind compact scheme. In the following section, using Fourier Analysis for dissipation and dispersion study to choose r_0, r_1, C^0, C^1, and C^2 will be discussed. C^0, C^1, and C^2 are the parametric weights for this seventh-order parametric weighted upwind compact scheme.

2.4 Eighth-Order Weighted Central Compact Scheme

Similarly as section 2.3, Seventh-Order Parametric Weighted Central Compact Scheme, three third-order approximations of the linear compact combination of numerical fluxes at $\hat{F}_{j-\frac{3}{2}}$, $\hat{F}_{j-\frac{1}{2}}$, $\hat{F}_{j+\frac{1}{2}}$, $\hat{F}_{j+\frac{3}{2}}$ and $\hat{F}_{j+\frac{5}{2}}$ are obtained from the three candidate stencils (Figure 2-1):

$$E^0_{WCCS} = \{F_{j-2}, F_{j-1}, F_j\}$$

$$E^1_{WCCS} = \{F_{j-1}, F_j, F_{j+1}\}$$

$$E^2_{WCCS} = \{F_j, F_{j+1}, F_{j+2}\}$$

Choosing the Lagrange polynomial for the third order approximation of linear combination of $\hat{F}_{j-\frac{3}{2}}$, $\hat{F}_{j-\frac{1}{2}}$, and $\hat{F}_{j+\frac{1}{2}}$, we obtain, for the first stencil E^0_{WCCS}:

$$\frac{3}{10}\hat{F}_{j-\frac{3}{2}} + \frac{13}{5}\hat{F}_{j-\frac{1}{2}} + \hat{F}_{j+\frac{1}{2}} \approx (\frac{5}{4}F_{j-1} + \frac{53}{20}F_j)/h \tag{2.14}$$

And similarly for the other two stencils $E^1_{WCCS}$and E^2_{WCCS}:

$$\frac{1}{4}\hat{F}_{j-\frac{1}{2}} + \hat{F}_{j+\frac{1}{2}} + \frac{1}{4}\hat{F}_{j+\frac{3}{2}} \approx (\frac{3}{4}F_j + \frac{3}{4}F_{j+1})/h \tag{2.15}$$

$$\hat{F}_{j+\frac{1}{2}} + \frac{13}{5}\hat{F}_{j+\frac{3}{2}} + \frac{3}{10}\hat{F}_{j+\frac{5}{2}} \approx (\frac{53}{20}F_{j+1} + \frac{5}{4}F_{j+2})/h \tag{2.16}$$

And

$$C^0_{WCCS} = \frac{5}{54} \qquad C^1_{WCCS} = \frac{44}{54} \qquad C^2_{WCCS} = \frac{5}{54}$$

will keep

$C^0_{WCCS}E^0_{WCCS} + C^1_{WCCS}E^1_{WCCS} + C^2_{WCCS}E^2_{WCCS}$ 8th order accuracy.

Then $\omega^0_{WCCS}E^0_{WCCS} + \omega^1_{WCCS}E^1_{WCCS} + \omega^2_{WCCS}E^2_{WCCS}$ is defined as 8th order Weighted Central Scheme with

$$\omega^{i,j\pm\frac{1}{2}}_{WCCS} = \frac{\gamma^{i,j\pm\frac{1}{2}}_{WCCS}}{\sum_{k=0}^{2}\gamma^{k,j\pm\frac{1}{2}}_{WCCS}} \qquad \gamma^{i,j\pm\frac{1}{2}}_{WCCS} = \frac{C^i_{WCCS}}{(\varepsilon + IS_{i,j\pm\frac{1}{2}})^p} \qquad i = 0,1,2$$

Acturally, this 8th Order Weighted Central Compact Scheme is a special case of 7th Order Parametric Weighted Upwind Compact Scheme. In next section, another special case of 7th Order Parametric Weighted Upwind Compact Scheme will be found as part of final WUCS.

2.5 Fourier Analysis of Truncation Error

Sanjiva K. Lele used Fourier analysis for compact scheme's dissipation and dispersion study in 1991 [25]. The use of Fourier analysis to characterize the errors of difference approximations is described extensively in [28]. It is a classical technique for

comparing differencing schemes. Fourier analysis of the standard Pad scheme was presented in [29] and comparisons were made with the second- and fourth-order central differences [25]. The Fourier analysis provides an effective way to quantify the resolution characteristics of the differencing approximations. This quantification will be used in later sections for constructing Weighted Upwind Compact Scheme. In the following section the differencing errors are analyzed in terms of dispersion and dissipation.

For the purposes of Fourier analysis the dependent variables are assumed to be periodic over the domain $[0, L]$ of the independent variable, i.e., $f_1 = f_{N+1}$ and $h = L/N$. The dependent variables may be decomposed into their Fourier coefficients

$$f(x) = \sum_{k=-\frac{N}{2}}^{\frac{N}{2}} \widehat{f_k} \mathrm{Exp}(\frac{2\pi i k x}{L}) \tag{2.17}$$

where $i = \sqrt{-1}$. Since the dependent variables are real-values, the Fourier coefficients satisfy $\hat{f}_k = \hat{f}_{-k}$ for $1 \leq k \leq \frac{N}{2}$ and $\widehat{f_0} = \overline{\widehat{f_0}}$, where $^-$ denotes the complex conjugate [25].

It is convenient to introduce a scaled wave number $w = \frac{2\pi k h}{L} = \frac{2\pi k}{N}$ and a scaled coordinate $s = \frac{x}{h}$. The Fourier modes in terms of these are simply $\mathrm{Exp}(iws)$. The domain of the scaled wavenumber w is $[\,0, \pi]$. The exact first derivative of (2.17) (with respect to s) generates a function with Fourier coefficients $\hat{f}'_k = iw\,\widehat{f_k}$. The differencing error of the first derivative scheme may be assessed by comparing the Fourier coefficients of the derivative obtained from the differencing scheme $(\hat{f}'_k)_{fd}$ with the exact Fourier coefficients $\hat{f}'_k$. Each finite difference scheme corresponds to a particular function $w'(w)$. Exact differentiation corresponds to the straight line $w' = w$. The range of wavenumbers The modified wavenumber $[\,2\pi/\mathrm{N}, w_f]$ over which the modified wavenumber $w'(w)$

approximates the exact differentiation $w'(w) = w$ within a specified error tolerance defines the set of well-resolved waves. w' corresponding to is in general complex. The real part of w', indicated by w'_r is associated with the dispersive error (when different from w) and the imaginary part, w'_i, is associated with the dissipative error [25].

2.5.1 Left Stencil

E^0 is represented by (2.9). This section E^0 's dispersion and dissipation will be listed.

$$w'_r = \frac{\begin{pmatrix}(10 + 4{t_0}^2 + 2t_0(-5 + t_1) + t_1(-1 + 4t_1) - (9 + t_0 + (-8 + t_1)t_1 \\ -2t_0(7 + 2t_1))\mathrm{Cos}(w) + (2 + 2t_0 - t_1)\mathrm{Cos}(2w))\mathrm{Sin}(w)\end{pmatrix}}{3(1 + {t_0}^2 + {t_1}^2 + 2(1 + t_0)t_1\mathrm{Cos}(w) + 2t_0\mathrm{Cos}(2w))}$$

$$w'_i = -\frac{4(-1 + {t_0}^2 - (-4 + t_1)t_1 + (4 + 4t_0 - 2t_1)\mathrm{Cos}(w))\mathrm{Sin}(\frac{w}{2})^4}{3(1 + {t_0}^2 + {t_1}^2 + 2(1 + t_0)t_1\mathrm{Cos}(w) + 2t_0\mathrm{Cos}(2w))}$$

2.5.2 Center Stencil

E^1 is represented by (2.10). This section E^1 's dispersion and dissipation will be listed.

$$w'_r = \frac{\begin{pmatrix}(-4 + s_1 - 2(s_0 + 2{s_0}^2 - 5s_0s_1 + 5s_1) + (1 + {s_0}^2 - 2s_0(2 + 7s_1) \\ +s_1(-8 + 9s_1))\mathrm{Cos}(w) + (1 - 2s_0 - 2s_1)s_1\mathrm{Cos}(2w))\mathrm{Sin}(w)\end{pmatrix}}{-3(1 + {s_0}^2 + {s_1}^2 + 2(s_0 + s_1)\mathrm{Cos}(w) + 2s_0s_1\mathrm{Cos}(2w))}$$

$$w'_i = -\frac{4(-1 + {s_0}^2 - (-4 + s_1)s_1 + 2s_1(-1 + 2s_0 + 2s_1)\mathrm{Cos}(w))\mathrm{Sin}(\frac{w}{2})^4}{3(1 + {s_0}^2 + {s_1}^2 + 2(s_0 + s_1)\mathrm{Cos}(w) + 2s_0s_1\mathrm{Cos}(2w))}$$

2.5.3 Right Stencil

E^2 is represented by (2.11). This section E^2 's dispersion and dissipation will be listed.

$$w'_r = \frac{\begin{pmatrix}(-2(2 + r_0 + 2{r_0}^2) + (10 + r_0)r_1 - 10{r_1}^2 + (1 + {r_0}^2 - 4r_0(1 + 2r_1) \\ +r_1(-14 + 9r_1))\mathrm{Cos}(w) + (-2 + r_0 - 2r_1)r_1\mathrm{Cos}(2w))\mathrm{Sin}(w)\end{pmatrix}}{-3(1 + {r_0}^2 + {r_1}^2 + 2r_0(1 + r_1)\mathrm{Cos}(w) + 2r_1\mathrm{Cos}(2w))}$$

$$w'_i = \frac{4(-1 + {r_0}^2 - 4r_0r_1 + {r_1}^2 + 2r_1(r_0 - 2(1 + r_1))\mathrm{Cos}(w))\mathrm{Sin}(\frac{w}{2})^4}{3(1 + {r_0}^2 + {r_1}^2 + 2r_0(1 + r_1)\mathrm{Cos}(w) + 2r_1\mathrm{Cos}(2w))}$$

2.6 Combination Methodology

Switching C^0, $C^1$and C^2 with ω^0, ω^1, and ω^2, weighted combination is formed as $\omega^0 E^0 + \omega^1 E^1 + \omega^2 E^2$. For seventh-order weighted upwind compact scheme, left stencil E^0 or center stencil E^1 will be used at where shock is developing. And right stencil E^2 will be dropped at shock. Because left stencil E^0 or center stencil E^1 is at upwind position, right stencil E^2 is at downwind position. For keeping seventh-order weighted upwind compact scheme stable, making left stencil E^0 and center stencil E^1 both have positive dissipation is necessary. The other necessary condition is that both left stencil E^0 and center stencil E^1 dispersive error cannot be too large, otherwise numerical oscillation in solution will be obvious.

2.6.1 Combination Requirements for Left Stencil

Based on 2.5.1, a positive dissipation condition is enforced as below. For $= \pi$, a lower bond of dissipation is given. And a upper bond of dissipation is given for $w = 3$. A dispersion upper bound at $w = 2.96$ is also listed below.

$$\begin{cases} -\dfrac{4(-1+{t_0}^2-(-4+t_1)t_1+(4+4t_0-2t_1)\mathrm{Cos}(w))\mathrm{Sin}(\frac{w}{2})^4}{3(1+{t_0}^2+{t_1}^2+2(1+t_0)t_1\mathrm{Cos}(w)+2t_0\mathrm{Cos}(2w))}\Big|_{w=\frac{3\pi}{4}} > 0 \\ -\dfrac{4(-1+{t_0}^2-(-4+t_1)t_1+(4+4t_0-2t_1)\mathrm{Cos}(w))\mathrm{Sin}(\frac{w}{2})^4}{3(1+{t_0}^2+{t_1}^2+2(1+t_0)t_1\mathrm{Cos}(w)+2t_0\mathrm{Cos}(2w))}\Big|_{w=\pi} > 6 \\ -\dfrac{4(-1+{t_0}^2-(-4+t_1)t_1+(4+4t_0-2t_1)\mathrm{Cos}(w))\mathrm{Sin}(\frac{w}{2})^4}{3(1+{t_0}^2+{t_1}^2+2(1+t_0)t_1\mathrm{Cos}(w)+2t_0\mathrm{Cos}(2w))}\Big|_{w=3} < 12 \\ \dfrac{\begin{pmatrix}(10+4{t_0}^2+2t_0(-5+t_1)+t_1(-1+4t_1)-(9+t_0+(-8+t_1)t_1)\\ -2t_0(7+2t_1))\mathrm{Cos}(w)+(2+2t_0-t_1)\mathrm{Cos}(2w))\mathrm{Sin}(w)\end{pmatrix}}{3(1+{t_0}^2+{t_1}^2+2(1+t_0)t_1\mathrm{Cos}(w)+2t_0\mathrm{Cos}(2w))}\Big|_{w=2.96} < 8 \end{cases}$$

2.6.2 Combination Requirements for Center Stencil

Comparing with 2.6.1 Left Stencil, a lower positive dissipation bond is given for Center Stencil, and more restrict dispersion requirement is enforced as below.

$$\begin{cases} -\dfrac{4(-1+{s_0}^2-(-4+s_1)s_1+2s_1(-1+2s_0+2s_1)\mathrm{Cos}(w))\mathrm{Sin}(\frac{w}{2})^4}{3(1+{s_0}^2+{s_1}^2+2(s_0+s_1)\mathrm{Cos}(w)+2s_0s_1\mathrm{Cos}(2w))}\Big|_{w=2.1} & >0 \\ -\dfrac{4(-1+{s_0}^2-(-4+s_1)s_1+2s_1(-1+2s_0+2s_1)\mathrm{Cos}(w))\mathrm{Sin}(\frac{w}{2})^4}{3(1+{s_0}^2+{s_1}^2+2(s_0+s_1)\mathrm{Cos}(w)+2s_0s_1\mathrm{Cos}(2w))}\Big|_{w=3.1} & >0.4 \\ \dfrac{\left(\begin{matrix}(-4+s_1-2(s_0+2{s_0}^2-5s_0s_1+5s_1)+(1+{s_0}^2-2s_0(2+7s_1)\\ +s_1(-8+9s_1))\mathrm{Cos}(w)+(1-2s_0-2s_1)s_1\mathrm{Cos}(2w))\mathrm{Sin}(w)\end{matrix}\right)}{-3(1+{s_0}^2+{s_1}^2+2(s_0+s_1)\mathrm{Cos}(w)+2s_0s_1\mathrm{Cos}(2w))}\Big|_{w=1.8} & <1.85 \end{cases}$$

2.6.3 Combination Results

Combining 2.4.1 and 2.4.2 with (2.12) , C^0, C^1, C^2, r_0, and r_1 can be chose as

$$C^0=\frac{1}{20} \qquad C^1=\frac{11}{20} \qquad C^2=\frac{2}{5} \qquad r_0=\frac{53}{80} \qquad r_1=\frac{-1}{100} \tag{2.18}$$

From this section, PWUCS will be used to identify a Parametric Weighted Upwind Compact Scheme with fixed parameters as (2.9), (2.10), (2.11), (2.12), (2.13) and (2.18).

2.7 Construction of WUCS by 7th PWUCS and 8th WCCS

As mentioned in Chapter 1, a fixed share or a fixed ratio of two different scheme for combination is more stable than a dynamic ratio of two different scheme. The other concern for combination is that using as more 8th WCCS as possible will benefit final WUCS for higher accuracy. The last and the most important combination condition, is that combined scheme should always keep positive dissipation for left stencil and center stencil.

Easy to see that, 8th Order WCCS can be derived from 7th order Parametric Weighted Upwind Compact Scheme by choosing specific parameters. Such as in (2.12),

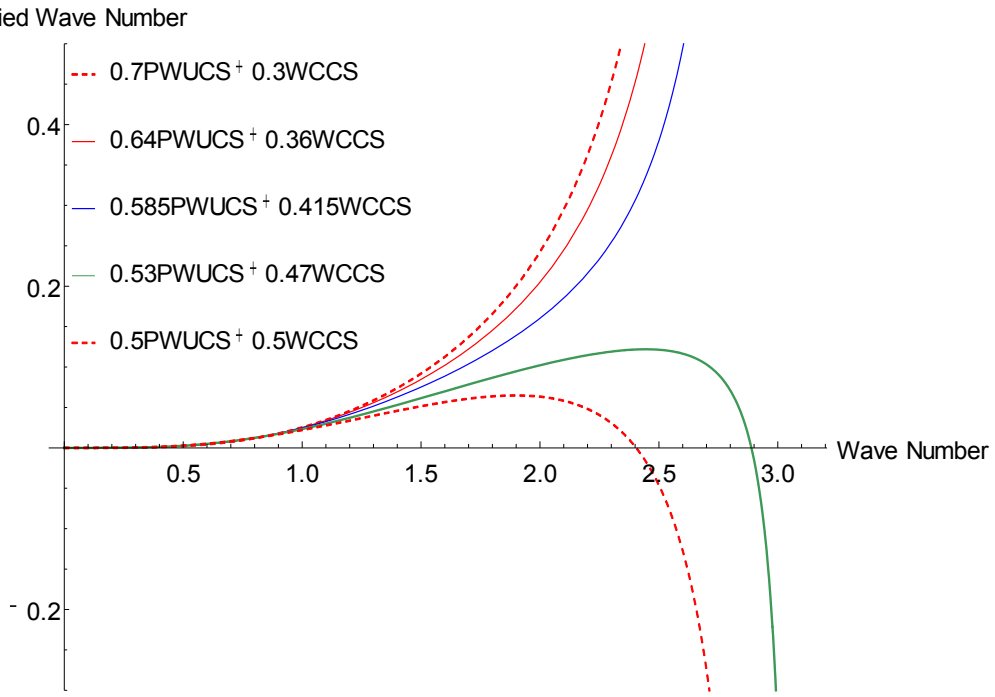

Figure 2-2 Im(w') for Left Stencil Combination

Making

$$C^0 = \frac{5}{54}, C^1 = \frac{22}{27}, C^2 = \frac{5}{54}, r_0 = \frac{13}{5}, r_1 = \frac{3}{10}$$

Then

$$t_0 = \frac{3}{10}, t_1 = \frac{13}{5}, s_0 = \frac{1}{4}, s_1 = \frac{1}{4}$$

and $E^i_{WCCS} = E^i_{WCCS}$ (i =1,2,3).

After several combination have been tested, a final combination of 58.5% 7th PWUCS and 41.5% 8th WCCS is a good compromise for keeping positive dissipation for left stencil and utilizing more 8th WCCS as possible. That is

$$0.585 * (\omega^0 E^0 + \omega^1 E^1 + \omega^2 E^2) + 0.415 * (\omega^0_{WCCS} E^0_{WCCS} + \omega^1_{WCCS} E^1_{WCCS} + \omega^2_{WCCS} E^2_{WCCS})$$

The major reason to have 58.5% PWUCS is trying keep positive dissipation for Left Stencil when there is a shock, and the combined WUCS utilizing Left Stencil mostly.

From Figure 2-2, a negative dissipation will emerge when WUCS utilize a little bit less percentage of PWUCS.

And combination details will be elaborated in next Chapter.

Chapter 3

Order, Dissipation and Dispersion Analysis

In this Chapter, a detailed analysis of the local truncation errors, the dissipation and dispersion terms is done for the Weighted Upwind Compact Scheme. A Fourier analysis and an investigation near shocks and in smooth area are performed.

3.1 Local Truncation Error of 7th Order PWUCS

From (2.9), (2,10), (2.11) and 2.4.3, $C^0E^0 + C^1E^1 + C^2E^2$'s truncation error is

$$C^0(t_0\hat{F}_{j-3/2} + t_1\hat{F}_{j-1/2} + \hat{F}_{j+1/2} - (t_2F_{j-2} + t_3F_{j-1} + t_4F_j)/h) + C^1(s_0\hat{F}_{j-1/2} + \hat{F}_{j+1/2}$$
$$+ s_1\hat{F}_{j+3/2} - (s_2F_{j-1} + s_3F_j + s_4F_{j+1})/h) + C^2(\hat{F}_{j+1/2} + r_0\hat{F}_{j+3/2} + r_1\hat{F}_{j+5/2}$$
$$- (r_2F_j + r_3F_{j+1} + r_4F_{j+2})/h)$$

$$= \frac{1}{24}(\frac{123}{500} + \frac{11}{10}(-1 + s_0 + 3s_1) + \frac{1}{10}(3 + t_0 - t_1))h^3\frac{\partial^4F_j}{\partial x^4}$$
$$+ \frac{1}{120}(-\frac{43}{500} - \frac{11}{10}(-2 + 3s_0 + 3s_1) + \frac{1}{10}(-18 - 8t_0 + 7t_1))h^4\frac{\partial^5F_j}{\partial x^5}$$
$$+ \frac{1}{720}(-\frac{69}{125} + \frac{11}{10}(-5 + 8s_0 + 12s_1) + \frac{1}{10}(75 + 41t_0 - 32t_1))h^5\frac{\partial^6F_j}{\partial x^6}$$
$$+ \frac{-\frac{601}{250} - \frac{11}{5}(-5 + 9s_0 + 9s_1) + \frac{1}{5}(-135 - 86t_0 + 61t_1)}{5040}h^6\frac{\partial^7F_j}{\partial x^7}$$
$$+ \frac{-\frac{3051}{500} + \frac{33}{10}(-7 + 13s_0 + 15s_1) + \frac{3}{10}(301 + 215t_0 - 141t_1)}{40320}h^7\frac{\partial^8F_j}{\partial x^8}$$
$$+ \frac{-\frac{7401}{500} - \frac{33}{10}(-14 + 27s_0 + 27s_1) - \frac{3}{10}(966 + 752t_0 - 463t_1)}{362880}h^8\frac{\partial^9F_j}{\partial x^9} + O(h^9)$$

Combining (2.9), above formula become (2.19) as below

$$C^0(t_0\hat{F}_{j-3/2} + t_1\hat{F}_{j-1/2} + \hat{F}_{j+1/2} - (t_2F_{j-2} + t_3F_{j-1} + t_4F_j)/h) + C^1(s_0\hat{F}_{j-1/2} + \hat{F}_{j+1/2}$$
$$+ s_1\hat{F}_{j+3/2} - (s_2F_{j-1} + s_3F_j + s_4F_{j+1})/h) + C^2(\hat{F}_{j+1/2} + r_0\hat{F}_{j+3/2} + r_1\hat{F}_{j+5/2}$$
$$- (r_2F_j + r_3F_{j+1} + r_4F_{j+2})/h)$$

$$= -\frac{23}{30000}h^7\frac{\partial^8 F_j}{\partial x^8} + \frac{13}{37800}h^8\frac{\partial^9 F_j}{\partial x^9} + O(h^9)$$

The dissipation error and the dispersion error can be extracted from (2.19), which are respectively the even derivative terms and the odd derivative terms of (2.19)

Dissipation error:

$$E_{7^{th}\,PWUCS,dissip} = -\frac{23}{30000}h^7\frac{\partial^8 F_j}{\partial x^8} + \cdots$$

Dispersion error:

$$E_{7^{th}\,PWUCS,disper} = \frac{13}{37800}h^8\frac{\partial^9 F_j}{\partial x^9} + \cdots$$

3.2 Local Truncation Error of 8th Order WCCS

From (2.14), (2.15), and (2.16), $C^0_{WCCS}E^0_{WCCS} + C^1_{WCCS}E^1_{WCCS} + C^2_{WCCS}E^2_{WCCS}$'s truncation error is

$$\frac{1}{420}h^8\frac{\partial^9 F_j}{\partial x^9} + O(h^{10})$$

Dissipation error:

$$E_{8^{th}\,WCCS,dissip} = 0$$

Dispersion error:

$$E_{8^{th}\,WCCS,disper} = \frac{1}{420}h^8\frac{\partial^9 F_j}{\partial x^9} + \cdots$$

3.3 Dissipation of Left Stencil

The dissipation error is associated with imaginary part of modified wave number w'.

For 8th Order WCCS Left Stencil,

$$w'_i = -\frac{91\mathrm{Sin}(w)^4}{25(\frac{157}{20} + \frac{169\mathrm{Cos}(w)}{25} + \frac{3}{5}\mathrm{Cos}(2w))}$$

For 7th Order PWUCS Left Stencil,

$$w'_i = -\frac{4(-\frac{8347}{375} - \frac{136\text{Cos}(w)}{25})\text{Sin}(\frac{w}{2})^4}{3(\frac{277997}{5625} + \frac{216172\text{Cos}(w)}{5625} - \frac{728}{75}\text{Cos}(2w))}$$

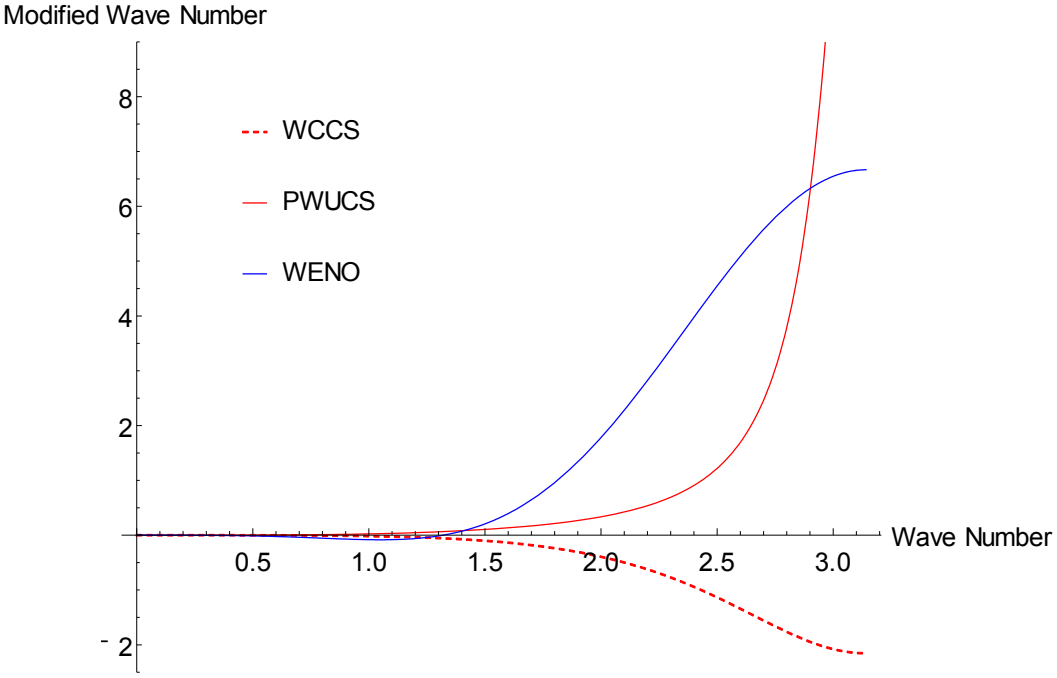

Figure 3-1 Im(w') of Left Stencil

For 5th Order WENO Left Stencil,

$$w'_i = \frac{4}{3}(1 - 4\text{Cos}(w))\text{Sin}(\frac{w}{2})^4$$

3.4 Dispersion of Left Stencil

The dispersion error is associated with the real part of the modified wave number.

For 8th Order WCCS Left Stencil,

$$w'_r = \frac{(\frac{834}{25} + \frac{1227\text{Cos}(w)}{100})\text{Sin}(w)}{3(\frac{157}{20} + \frac{169\text{Cos}(w)}{25} + \frac{3}{5}\text{Cos}(2w))}$$

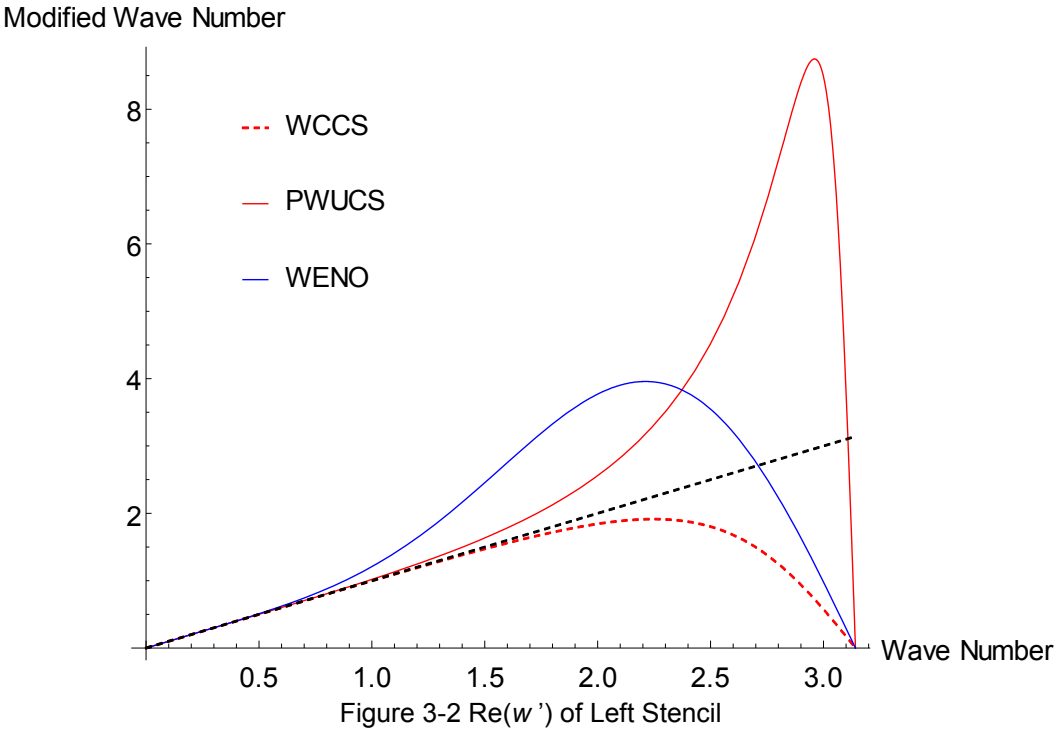

Figure 3-2 Re(w') of Left Stencil

For 7th Order PWUCS Left Stencil,

$$w'_r = -\frac{4\left(-\frac{8347}{375}-\frac{136\mathrm{Cos}(w)}{25}\right)\mathrm{Sin}\left(\frac{w}{2}\right)^4}{3\left(\frac{277997}{5625}+\frac{216172\mathrm{Cos}(w)}{5625}-\frac{728}{75}\mathrm{Cos}(2w)\right)}$$

For 5th Order WENO Left Stencil,

$$w'_r = \frac{4}{3}(1-4\mathrm{Cos}(w))\mathrm{Sin}\left(\frac{w}{2}\right)^4$$

Figure 3-1 and Figure 3-2 are very appreciable, if some scheme can have modified wave number between red line and red dash line, that would be a good compromise for both dissipation and dispersion. Actually, WUCS can make this compromise dynamically which will be introduced in 3.11.

3.5 Dissipation of Center Stencil

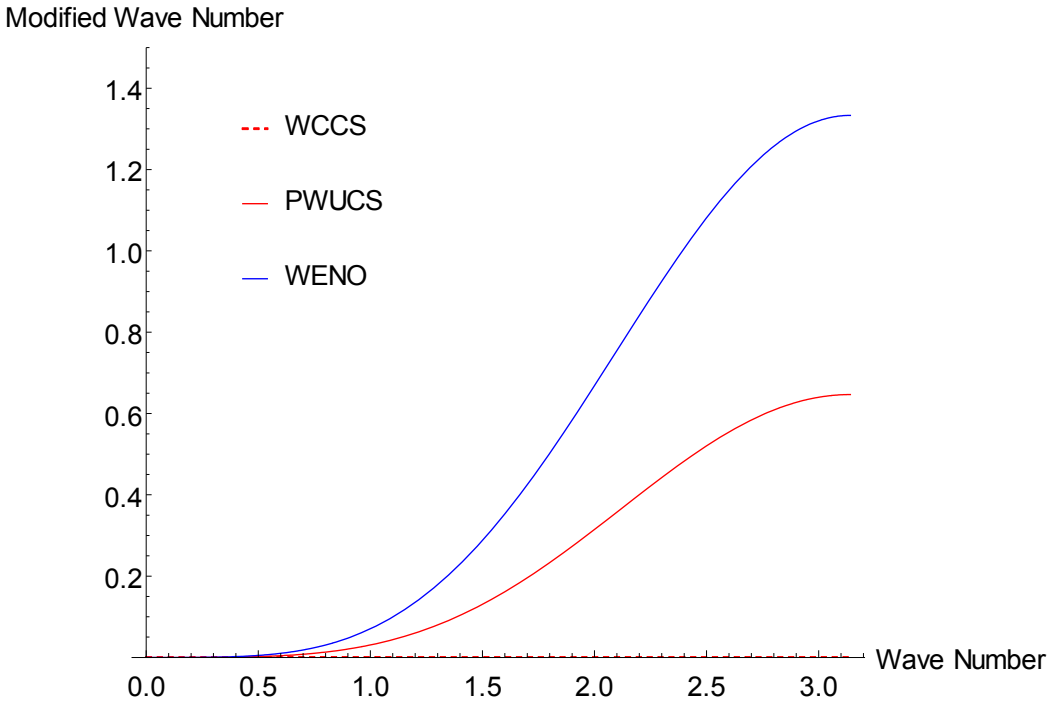

Figure 3-3 Im(w') of Center Stencil

Since 8th Order WCCS Center Stencil is a central compact scheme,

$$w'_i = 0$$

For 7th Order PWUCS Center Stencil,

$$w'_i = -\frac{4\left(-\frac{27737}{60500} - \frac{108088\mathrm{Cos}(w)}{680625}\right)\mathrm{Sin}\left(\frac{w}{2}\right)^4}{3\left(\frac{2790317}{2722500} + \frac{353\mathrm{Cos}(w)}{825} + \frac{14198\mathrm{Cos}(2w)}{680625}\right)}$$

For 5th Order WENO Center Stencil,

$$w'_i = \frac{4}{3}\mathrm{Sin}\left(\frac{w}{2}\right)^4$$

3.6 Dispersion of Center Stencil

For 8th Order WCCS Center Stencil,

$$w'_r = -\frac{(-\frac{9}{2} - \frac{9\mathrm{Cos}(w)}{4})\mathrm{Sin}(w)}{3(\frac{9}{8} + \mathrm{Cos}(w) + \frac{1}{8}\mathrm{Cos}(2w))}$$

For 7th Order PWUCS Center Stencil,

$$w'_r = -\frac{(-\frac{2805826}{680625} - \frac{1028899\mathrm{Cos}(w)}{2722500} + \frac{54044\mathrm{Cos}(2w)}{680625})\mathrm{Sin}(w)}{3(\frac{2790317}{2722500} + \frac{353\mathrm{Cos}(w)}{825} + \frac{14198\mathrm{Cos}(2w)}{680625})}$$

For 5th Order WENO Center Stencil,

$$w'_r = -\frac{1}{3}(-4 + \mathrm{Cos}(w))\mathrm{Sin}(w)$$

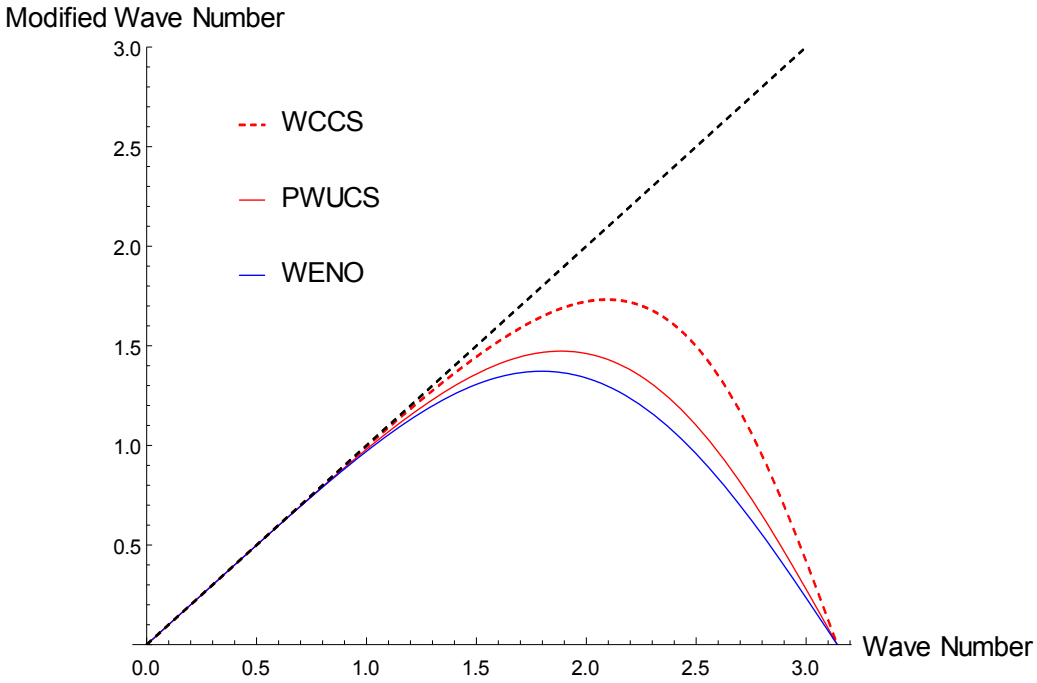

Figure 3-4 Re(w') of Center Stencil

3.7 Dissipation of Right Stencil

For 8th Order WCCS Right Stencil,

$$w'_i = \frac{91\mathrm{Sin}(\frac{w}{2})^4}{25(\frac{157}{20} + \frac{169\mathrm{Cos}(w)}{25} + \frac{3}{5}\mathrm{Cos}(w))}$$

For 7th Order PWUCS Right Stencil,

$$w'_i = \frac{4(-\frac{85519}{160000} + \frac{527\mathrm{Cos}(w)}{20000})\mathrm{Sin}(\frac{w}{2})^4}{3(\frac{230241}{160000} + \frac{5247\mathrm{Cos}(w)}{4000} - \frac{1}{50}\mathrm{Cos}(2w))}$$

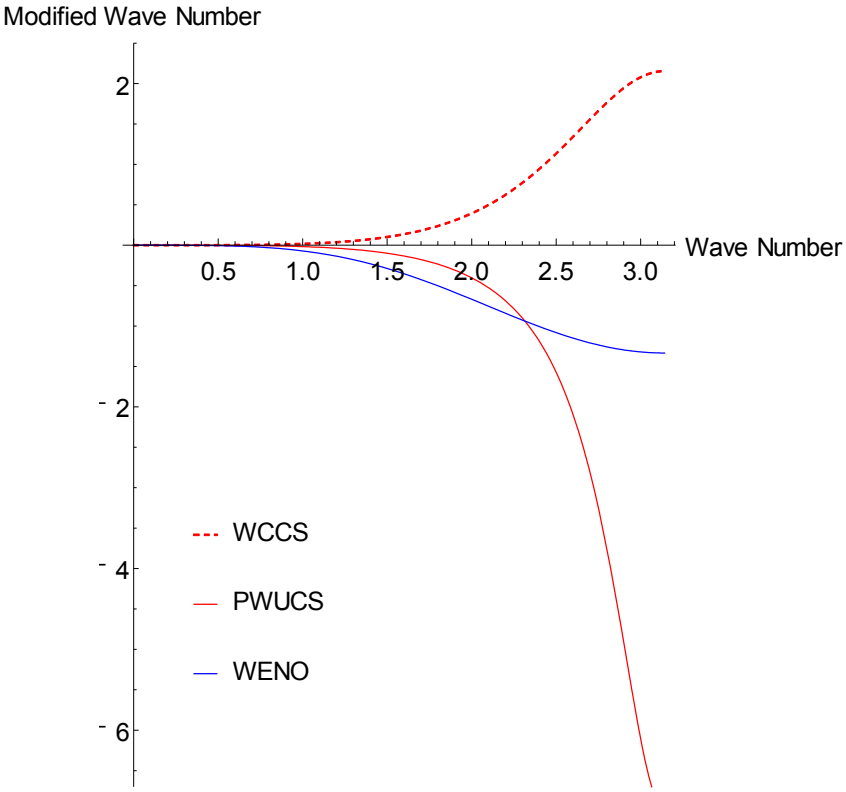

Figure 3-5 Im(w') of Right Stencil

For 5th Order WENO Right Stencil,

$$w'_i = -\frac{4}{3}\mathrm{Sin}(\frac{w}{2})^4$$

3.8 Dispersion of Right Stencil

For 8th Order WCCS Right Stencil,

$$w'_r = -\frac{(-\frac{834}{25} - \frac{1227\mathrm{Cos}(w)}{100})\mathrm{Sin}(w)}{3(\frac{157}{20} + \frac{169\mathrm{Cos}(w)}{25} + \frac{3}{5}\mathrm{Cos}(2w))}$$

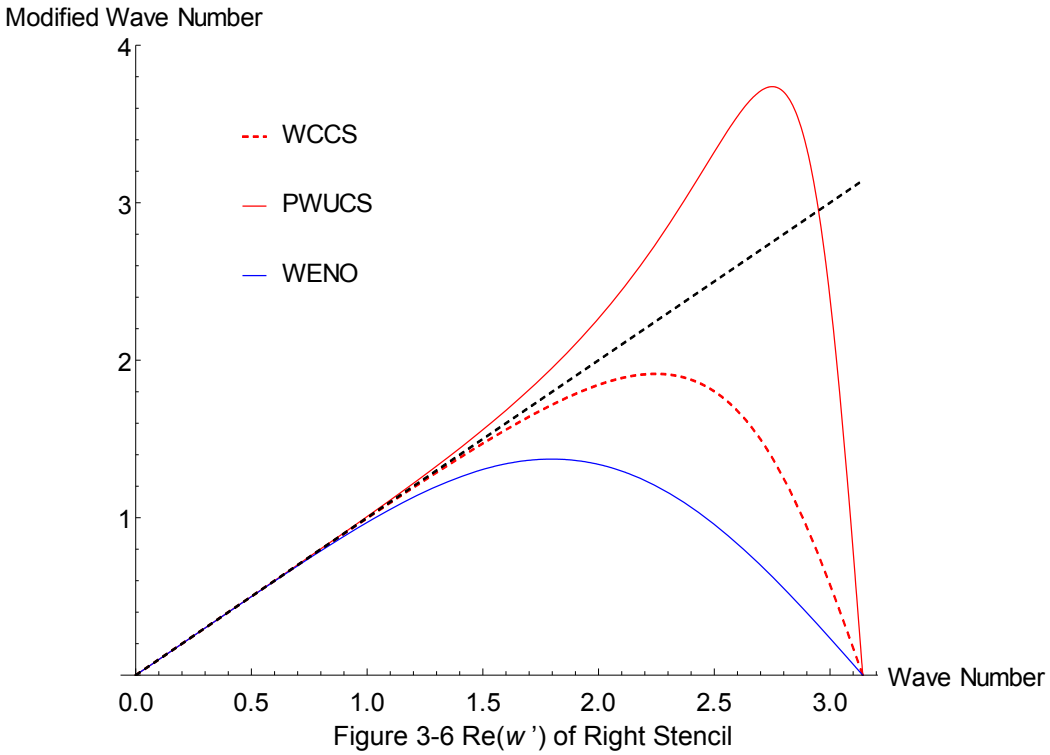

Figure 3-6 Re(*w* ') of Right Stencil

For 7th Order PWUCS Right Stencil,

$$w'_r = -\frac{(-\frac{28753}{4000} - \frac{162751\mathrm{Cos}(w)}{160000} + \frac{527\mathrm{Cos}(2w)}{40000})\mathrm{Sin}(w)}{3(\frac{230241}{160000} + \frac{5247\mathrm{Cos}(w)}{4000} - \frac{1}{50}\mathrm{Cos}(2w))}$$

For 5th Order WENO Right Stencil,

$$w'_r = -\frac{1}{3}(-4 + \mathrm{Cos}(w))\mathrm{Sin}(w)$$

3.9 Dissipation of Combined Scheme

For 8th Order WCCS,

$$w'_i = 0$$

For 7th Order PWUCS,

$$w'_i = -\frac{32\left(-\frac{3467}{375}+\frac{136\text{Cos}(w)}{125}\right)\text{Sin}\left(\frac{w}{2}\right)^8}{15\left(\frac{137101}{1125}+\frac{68416\text{Cos}(w)}{1875}+20\left(-\frac{9927\text{Cos}(2w)}{3125}-\frac{23062\text{Cos}(3w)}{28125}+\frac{91\text{Cos}(4w)}{9375}\right)\right)}$$

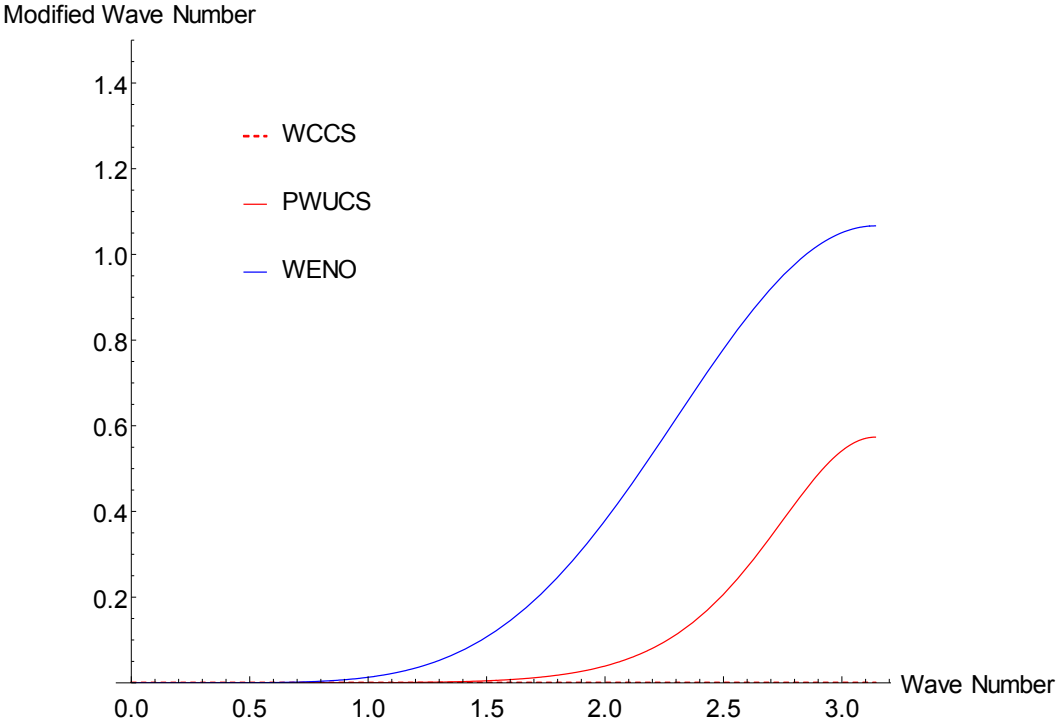

Figure 3-7 Im(w') of Combined Scheme

For 5th Order WENO,

$$w'_i = -\frac{4}{3}\text{Sin}\left(\frac{w}{2}\right)^4$$

3.10 Dispersion of Combined Scheme

For 8th Order WCCS,

$$w'_r = \frac{\frac{250000\text{Sin}(w)}{27}+\frac{432500}{81}\text{Sin}(2w)+\frac{70000}{81}\text{Sin}(3w)+\frac{3125}{81}\text{Sin}(4w)}{60\left(\frac{22625}{162}+\frac{14800\text{Cos}(w)}{81}+20\left(\frac{205}{81}\text{Cos}(2w)+\frac{20}{81}\text{Cos}(3w)+\frac{5}{648}\text{Cos}(4w)\right)\right)}$$

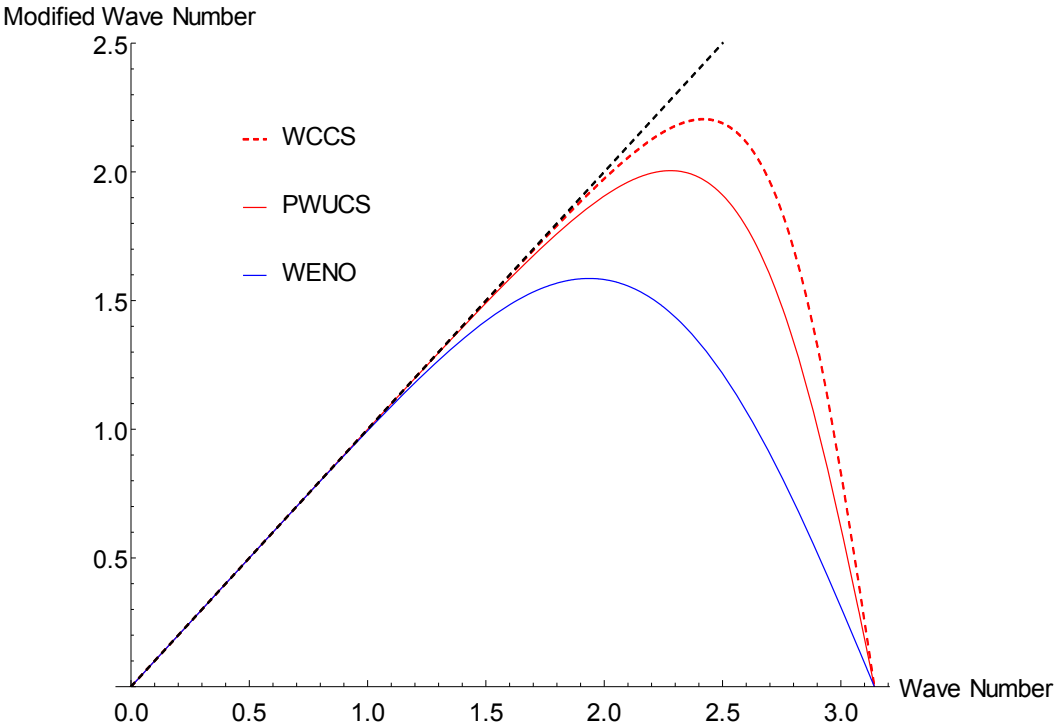

Figure 3-8 Re(w') of Combined Scheme

For 7th Order PWUCS,

$$w'_r = \frac{\frac{5582384\mathrm{Sin}(w)}{375} - \frac{485968}{375}\mathrm{Sin}(2w) - \frac{2759564\mathrm{Sin}(3w)}{1125} - \frac{6917}{125}\mathrm{Sin}(4w) + \frac{68}{125}\mathrm{Sin}(5w)}{60(\frac{137101}{1125} + \frac{68416\mathrm{Cos}(w)}{1875} + 20(-\frac{9927\mathrm{Cos}(2w)}{3125} - \frac{23062\mathrm{Cos}(3w)}{28125} + \frac{91\mathrm{Cos}(4w)}{9375}))}$$

For 5th Order WENO,

$$w'_r = \frac{1}{30}(45\mathrm{Sin}(w) - 9\mathrm{Sin}(2w) + \mathrm{Sin}(3w))$$

3.11 Left Stencil of WUCS

Though WUCS is a combination with 58.5% from PWUCS and 41.5% from WCCS, each Stencil is not combined by a constant share. For instance, Left Stencil of WUCS is a dynamic combination of 7th order PWUCS's Left Stencil and 8th order WCCS's Left Stencil. In smooth area, when $\omega^0 = 1/20$ for PWUCS's Left Stencil, $\omega^0_{WCCS} = 5/54$ for

WCCS's Left Stencil; around shock, when $\omega^0 = 1$ for PWUCS's Left Stencil, $\omega^0_{WCCS} = 1$ for WCCS's Left Stencil. In some intermediate area between smooth area and shock, when $\omega^0 = 1/12$ for PWUCS's Left Stencil, $\omega^0_{WCCS} = 5/49$ for WCCS's Left Stencil. The different dissipation properties can be shown as below

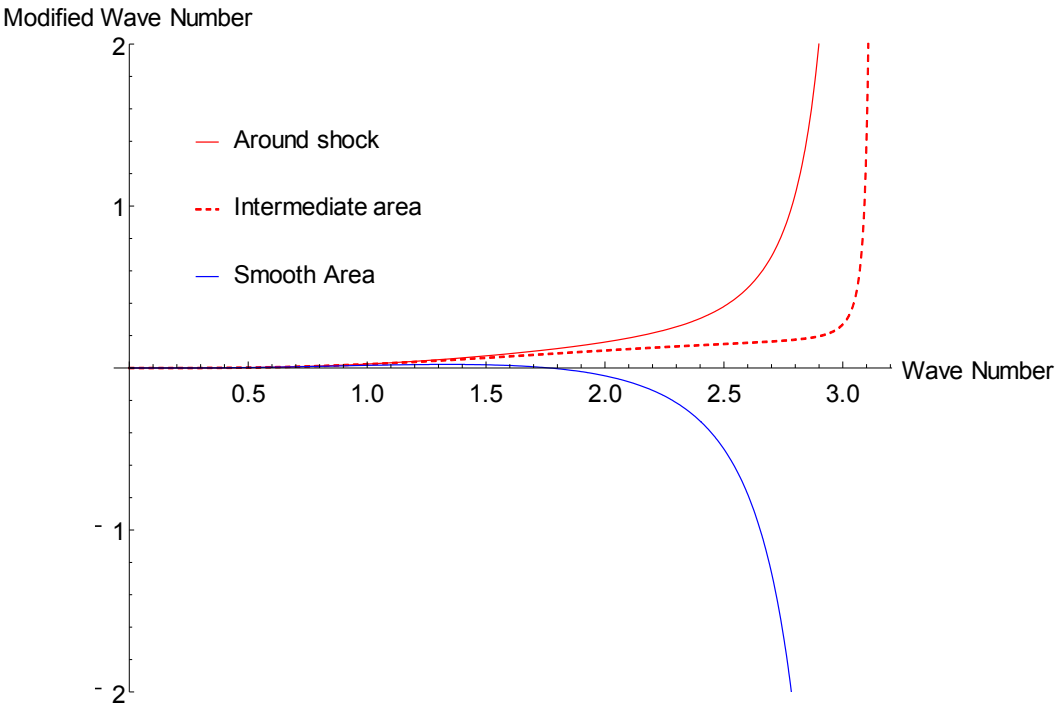

Figure 3-9 Im(w') of WUCS's Left Stencil

From Figure 3-9, an adaptive dissipation property is very clear for WUCS.

Chapter 4

1D and 2D cases for WUCS

In this Chapter, several selected one-dimensional and two-dimensional fluid dynamics cases will be used to testify previous chapters' deriving. All the cases' derivative solver is using WUCS.

4.1 Order test by One-Dimensional smooth functions

Firstly, order test results for PWUCS are tabulated in Table 4-1 and Table 4-3. It can show that PWUCS has expected 7^{th} order accuracy as section 3.1. After that, order test results for WUCS is tabulate in Table 4-2 and Table 4-3. It can testify that WUCS still keep 7^{th} order accuracy after the combination WCCS with PWUCS. In the following order test, p is chosen as 5, and ε is chosen to be 10^{-2} in accordance with (2.13).

4.1.1 PWUCS order test by Sin(πx)

$$f(x) = \mathrm{Sin}(\pi x) \qquad -1 \le x \le 1$$
$$f'(x) = \pi \mathrm{Cos}(\pi x) \qquad -1 \le x \le 1$$

Table 4-1 Errors of the numerical derivative of Sin(πx)

Grid Points	Error Infinity-Norm	Error Order	Error Two-Norm	Error Order
9	3.10E+00		3.37E+00	
17	1.25E-01	4.64	1.46E-01	4.54
33	2.96E-03	5.40	3.66E-03	5.31
65	4.40E-06	9.39	1.01E-05	8.50
129	2.55E-08	7.43	1.59E-07	5.99
257	2.39E-10	6.74	2.03E-09	6.29
513	2.06E-12	6.86	2.33E-11	6.44

4.1.2 *PWUCS order test by* $\mathrm{Sin}^2(\pi x)$

$$f(x) = \mathrm{Sin}^2(\pi x) \qquad -1 \le x \le 1$$
$$f'(x) = \pi \mathrm{Sin}(2\pi x) \qquad -1 \le x \le 1$$

Table 4-2 Errors of the numerical derivative of $\mathrm{Sin}^2(\pi x)$

Grid Points	Error Infinity-Norm	Error Order	Error Two-Norm	Error Order
9	1.04E+01		1.44E+01	
17	5.96E-01	4.13	6.91E-01	4.38
33	1.30E-02	5.51	2.04E-02	5.08
65	5.90E-05	7.79	2.76E-04	6.21
129	7.93E-07	6.22	5.16E-06	5.74
257	7.58E-09	6.71	6.86E-08	6.23
513	6.28E-11	6.92	7.99E-10	6.42

4.1.3 *WUCS order test by* $\mathrm{Sin}(\pi x)$

$$f(x) = \mathrm{Sin}(\pi x) \qquad -1 \le x \le 1$$
$$f'(x) = \pi \mathrm{Cos}(\pi x) \qquad -1 \le x \le 1$$

Table 4-3 Errors of the numerical derivative of $\mathrm{Sin}(\pi x)$

Grid Points	Error Infinity-Norm	Error Order	Error Two-Norm	Error Order
9	2.01E+00		2.18E+00	
17	8.21E-02	4.61	9.35E-02	4.54
33	3.01E-03	4.77	3.44E-03	4.76
65	4.33E-06	9.44	6.78E-06	8.99
129	1.05E-08	8.68	6.50E-08	6.70
257	9.74E-11	6.76	8.26E-10	6.30
513	9.77E-13	6.64	9.56E-12	6.43

4.1.4 *WUCS order test by* $\mathrm{Sin}^2(\pi x)$

$$f(x) = \mathrm{Sin}^2(\pi x) \qquad -1 \le x \le 1$$
$$f'(x) = \pi \mathrm{Sin}(2\pi x) \qquad -1 \le x \le 1$$

Table 4-4 Errors of the numerical derivative of $\mathrm{Sin}^2(\pi x)$

Grid Points	Error Infinity-Norm	Error Order	Error Two-Norm	Error Order
9	9.71E+00		1.30E+01	
17	3.03E-01	5.00	4.61E-01	4.82
33	1.01E-02	4.91	1.45E-02	4.99
65	2.83E-05	8.48	1.28E-04	6.83
129	3.39E-07	6.38	2.18E-06	5.87
257	3.12E-09	6.76	2.82E-08	6.27
513	2.57E-11	6.92	3.26E-10	6.44

Comparing Table 4-1, Table 4-2 with Table 4-3, Table 4-4, it can be noticed that WUCS has even smaller error than PWUCS. The reason is that the 8th order WCCS has been combined with PWUCS.

4.2 One-Dimensional Cases

The one-dimensional Euler equations in vector and conservative form read as

$$\frac{\partial U}{\partial t} + \frac{\partial F}{\partial x} = 0$$
$$U = (\rho, \rho u, E_t)^T \tag{4.1}$$
$$F = (\rho u, \rho u^2 + p, u(E_t + p))^T$$

Where $p = (\gamma - 1)(E - \rho u^2/2)$ with $\gamma = 1.4$ and the grid is uniform with 201 grid points for 4.2.1, 4.2.2 and 4.2.3, and another uniform grids with 401 grid points also tested for 4.2.2 and 4.2.3.

In this section, Steger-Warming flux-splitting method will be used for WUCS, and a fourth-order Runge-Kutta scheme will be used for time marching. In (4.1), ρ represents gas density, u represents velocity, E_t represents energy, and p represents pressure.

4.2.1 Sod Shock-Tube

The Sod shock tube problem, named after Gary A. Sod, which is a Riemann problem used as a standard one-dimensional case in computational fluid dynamics [32]. The initial conditions are very simple:

$$(\rho, u, p)^T = \begin{cases} (1,0,1) & t = 0, \quad -5 \le x \le 0 \\ (0.125,0,0.1) & t = 0, \quad 0 < x \le 5 \end{cases} \tag{4.2}$$

The fundamental idea of the shock tube is the following: consider a long one-dimensional (1D) tube, closed at its ends and divided into two equal regions by a thin diaphragm (see Figure 4-1). Each region is filled with the same gas, but with different thermodynamic parameters (pressure, density, and temperature). The region with the highest pressure is called the driven section of the tube, while the low-pressure part is the working section. The gas being initially at rest, the sudden breakdown of the diaphragm generates a high-speed flow, which propagates in the working section (this is the place where the model of a free-flying object, such as a supersonic aircraft, will be placed).

Figure 4-1 Initial Pressure Distribution of SOD Shock-Tube

Figures 4-2 and 4-3 report the velocity solution on the whole domain for WUCS and WENO schemes at time t = 2, respectively. Velocity solution from WUCS 201 results does not have overshooting in the whole domain.

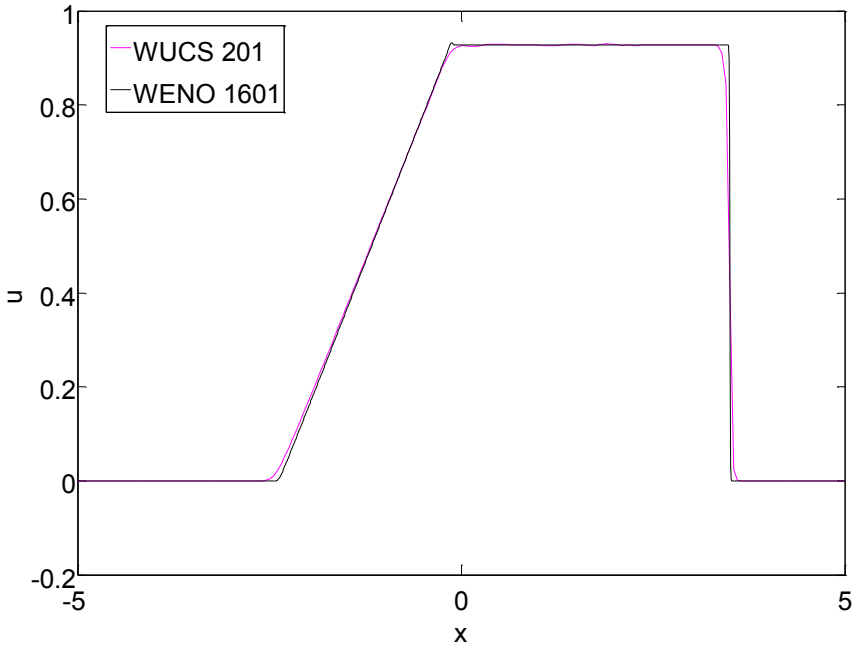

Figure 4-2 Velocity Solution from WUCS

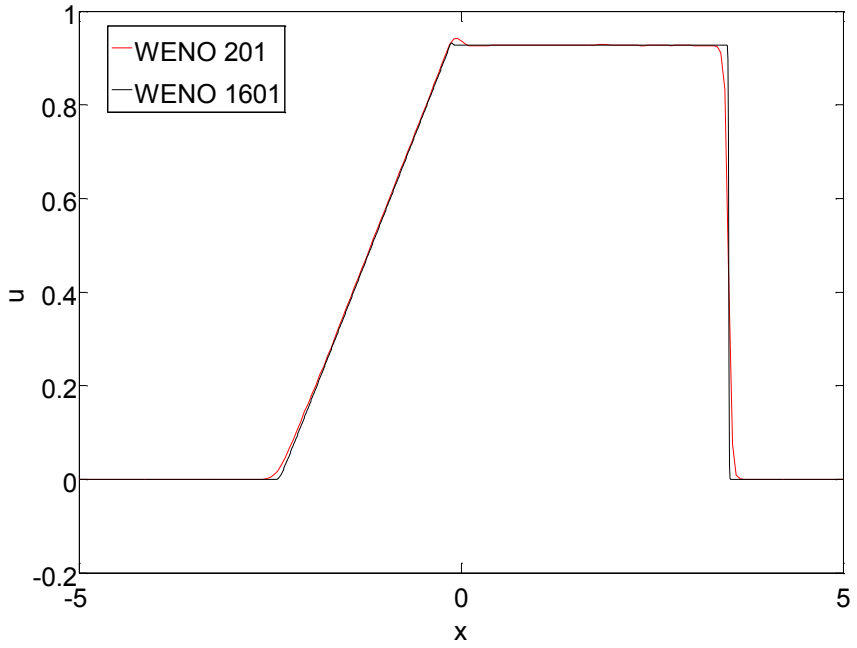

Figure 4-3 Velocity Solution from WENO

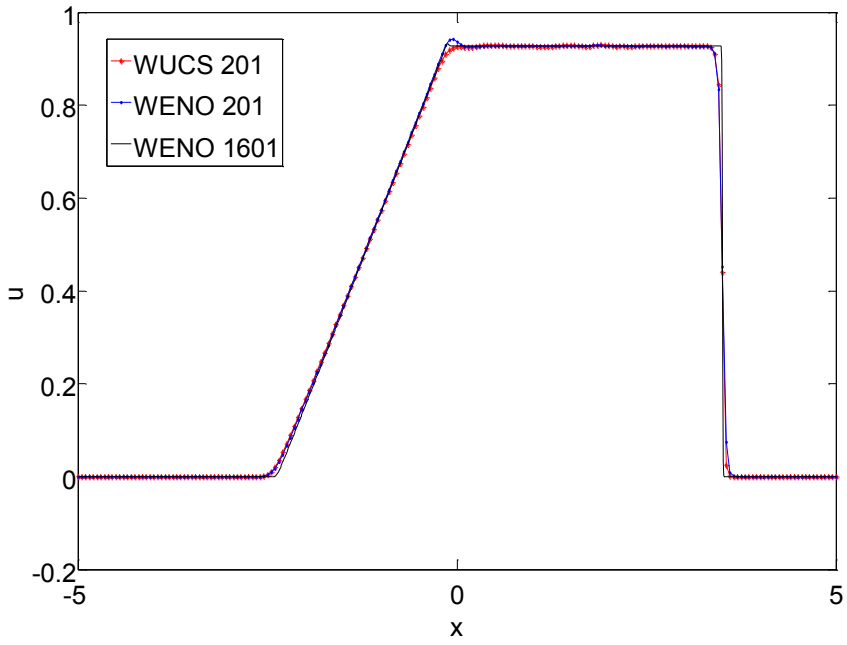

Figure 4-4 Comparison of velocity solution

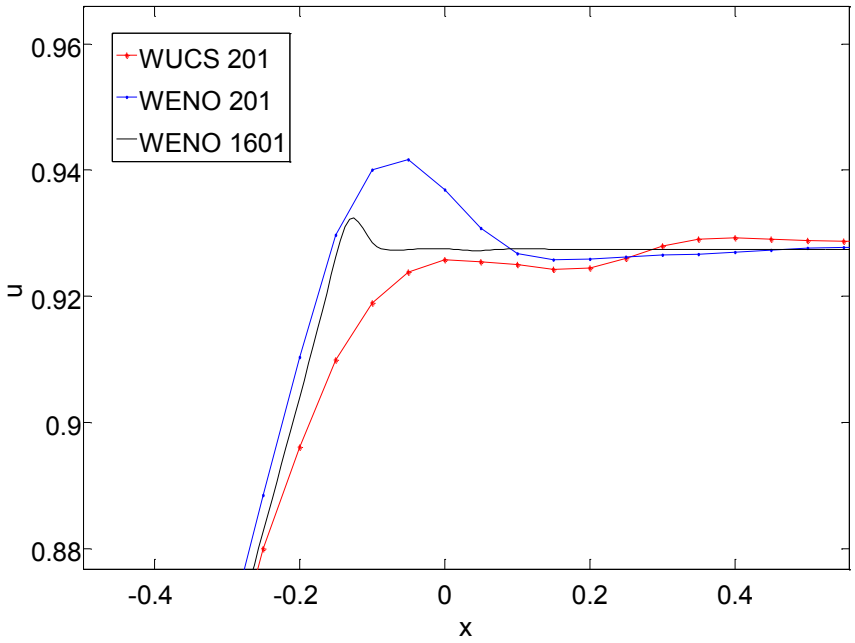

Figure 4-5 Enlargement of velocity solution

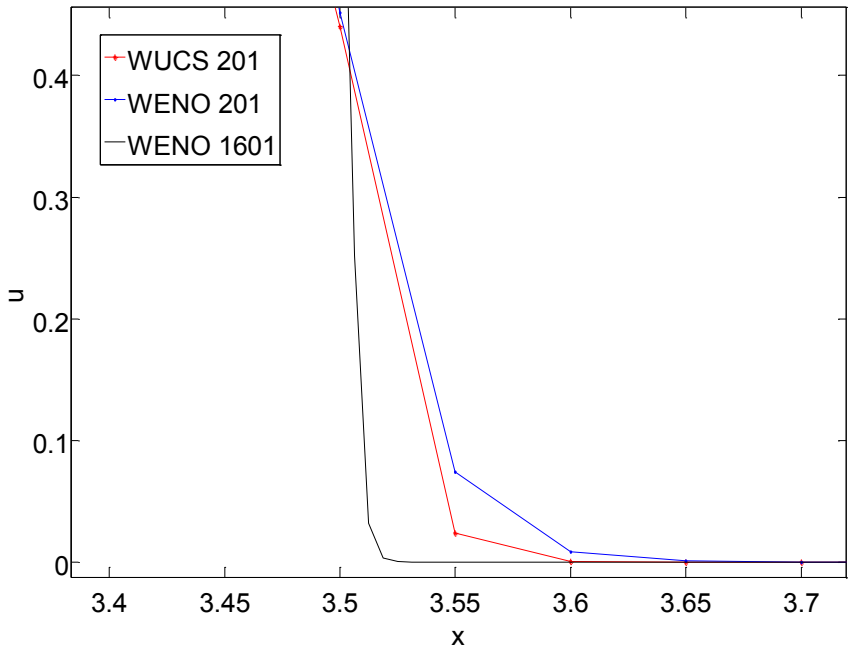

Figure 4-6 Enlargement of velocity solution

Figures 4-2, 4-3 and 4-4 report the velocity solution on the whole domain for WUCS and WENO schemes at time t = 2, respectively. Figures 4-5 and 4-6 show the enlargement plots of the solved velocity u, at time t = 2 from both WUCS and WENO. The reference solution is regarded as the one obtained by the fifth-order WENO scheme using a mesh of 1601 points, labeled as WENO 1601. The other two simulations are carried out on a coarser mesh of 201 points. The solutions using WUCS (labeled as WUCS 201) and WENO scheme (labeled as WENO 201) are free from visible oscillations. Figure 4-6 reports an enlargement of the downstream shock area, comparing the two different schemes. Using WUCS scheme, the discontinuity is captured more sharply and is less smeared compared to the fifth-order WENO.

4.2.2 Shu-Osher Problem

The Shu-Osher problem simulates a normal shock front moving inside a one-dimensional inviscid flow with artificial density fluctuations. In Shu-Osher problem, the computation domain is $x \in [-5, 5]$. The downstream flow is assumed to have a sinusoidal density fluctuation $\rho = 1 + 0.2 * \mathrm{Sin}(5x)$ with a wave length of $2\pi/5$ and an amplitude of 1/5. *A* normal shock front with a Mach number of 3.0 is initially placed at the position $x = -4$. The initial conditions for the simulation are

$$(\rho, u, p)^T = \begin{cases} (3.857143, 2.629369, 10.33333) & t = 0, \quad x < -4 \\ (1 + 0.2 * \mathrm{Sin}(5x), 0, 1) & t = 0, \quad x \geq -4 \end{cases} \tag{4.3}$$

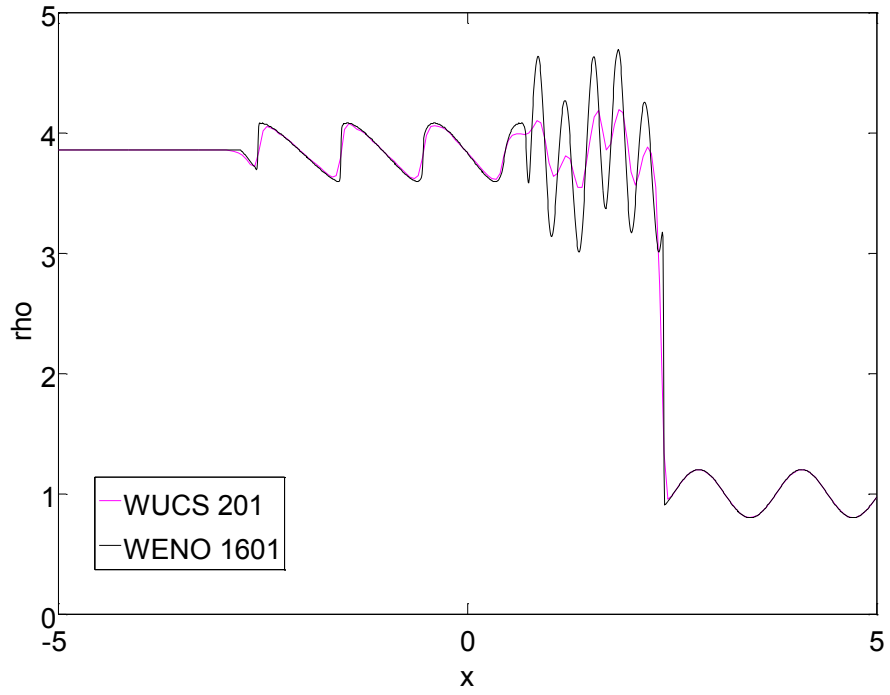

Figure 4-7 Density Solution of Shu-Osher Problem from WUCS

The shock-entropy wave interaction problem (Shu and Osher, Efficient implementation of essentially non-oscillatory shock-capturing schemes II 1989) is solved in order to test the proposed method's capability on shock-capturing and shock-

turbulence interaction. The entropy waves are very sensitive to numerical dissipation introduced by a numerical scheme, and can be excessively damped.

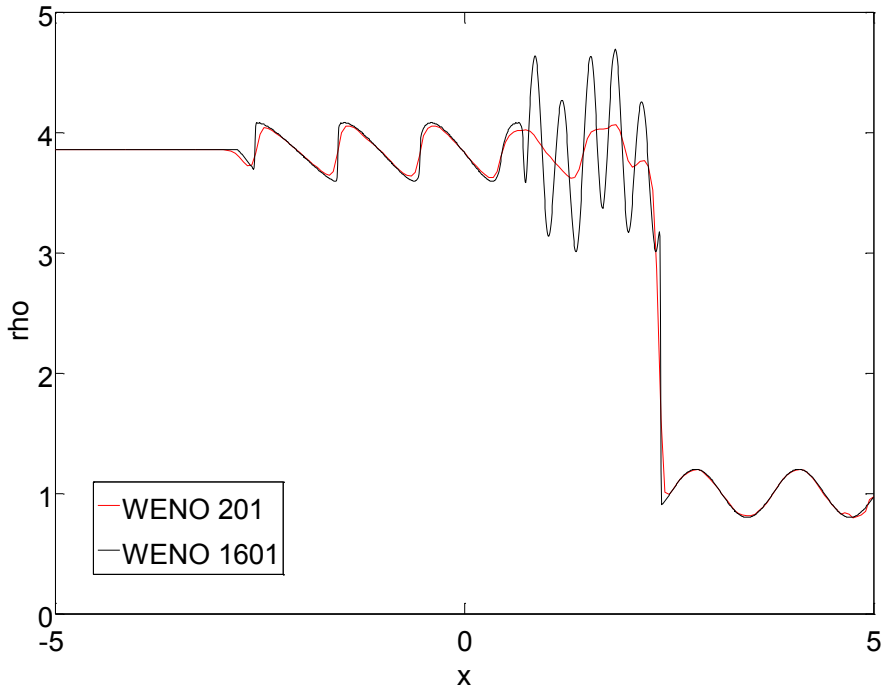

Figure 4-8 Density Solution of Shu-Osher Problem from WENO

Figures 4-7 and 4-8 show the result of the solved density distribution at time t = 1.8 on the whole domain for WUCS, and WENO schemes, respectively. Figure 4-9 show the comparison of the Shu-Osher density solution from WUCS and WENO. Same as in section 4.2.1, the reference solution is regarded as the one obtained by the fifth-order WENO scheme using a mesh of 1601 points, labeled as WENO 1601. All the other calculations are made on a coarser mesh of 201 points. The WUCS scheme (labeled WUCS 201) shows higher resolution and sharper shock capturing compared to WENO (labeled WENO 201).

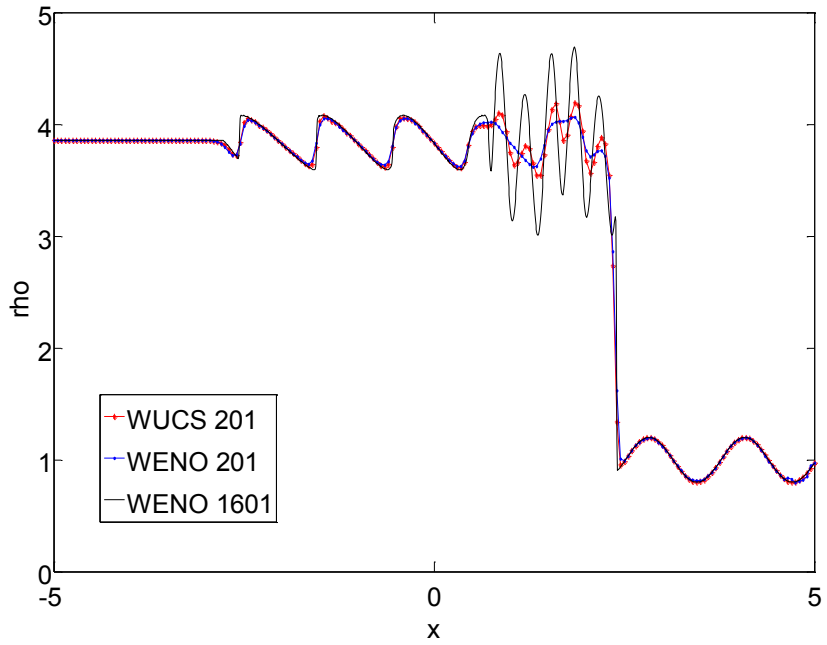

Figure 4-9 Density solution of Shu-Osher problem

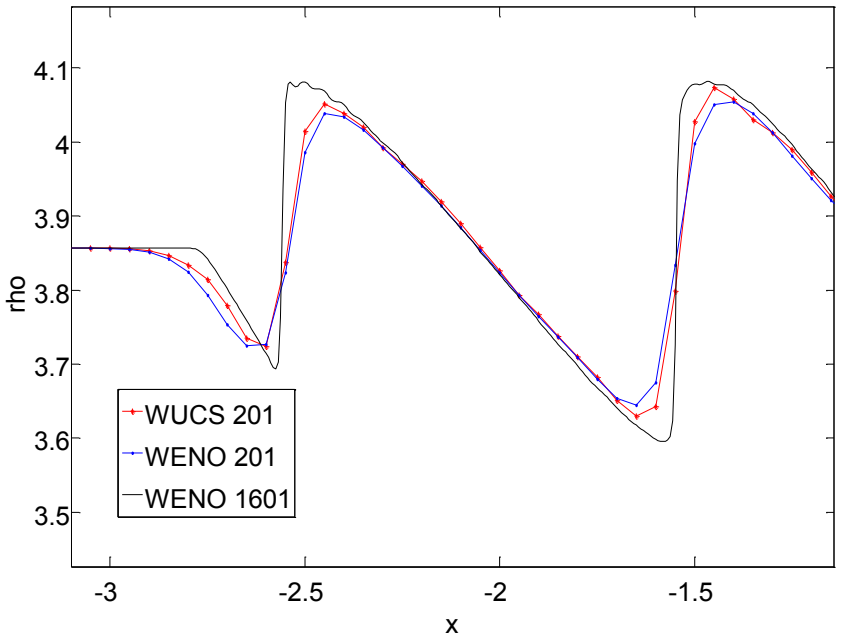

Figure 4-10 Enlargement of density solution of Shu-Osher problem

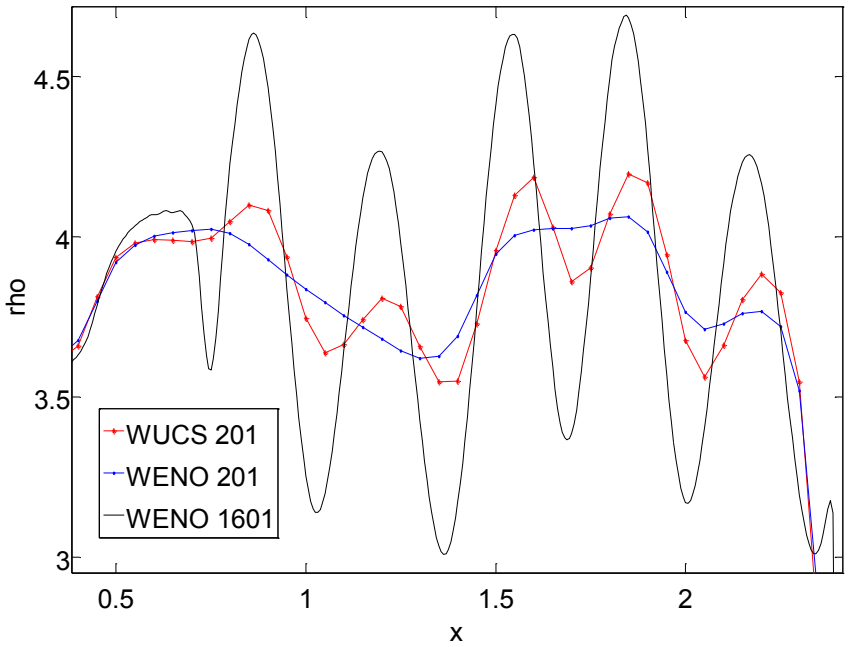

Figure 4-11 Enlargement of density solution of Shu-Osher problem

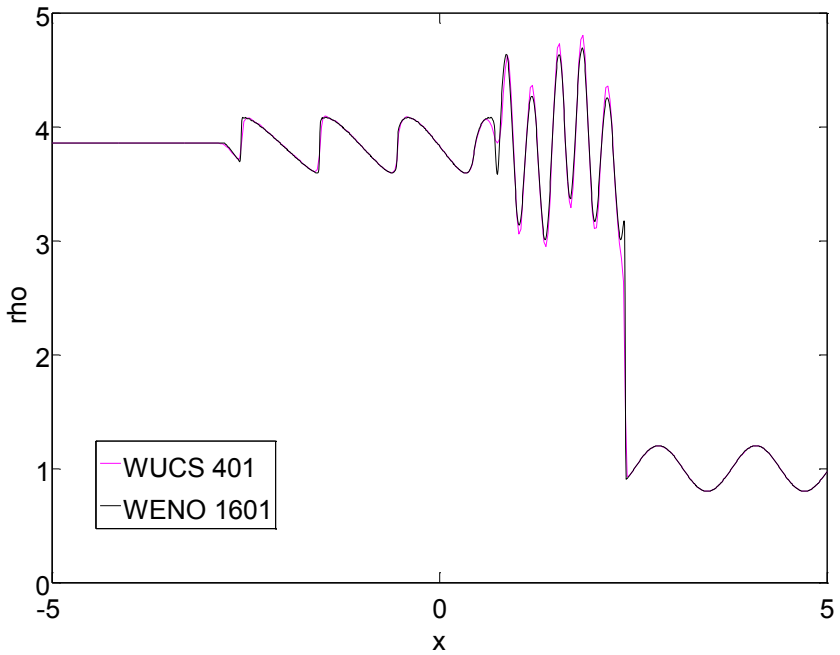

Figure 4-12 Density Solution of Shu-Osher Problem from WUCS

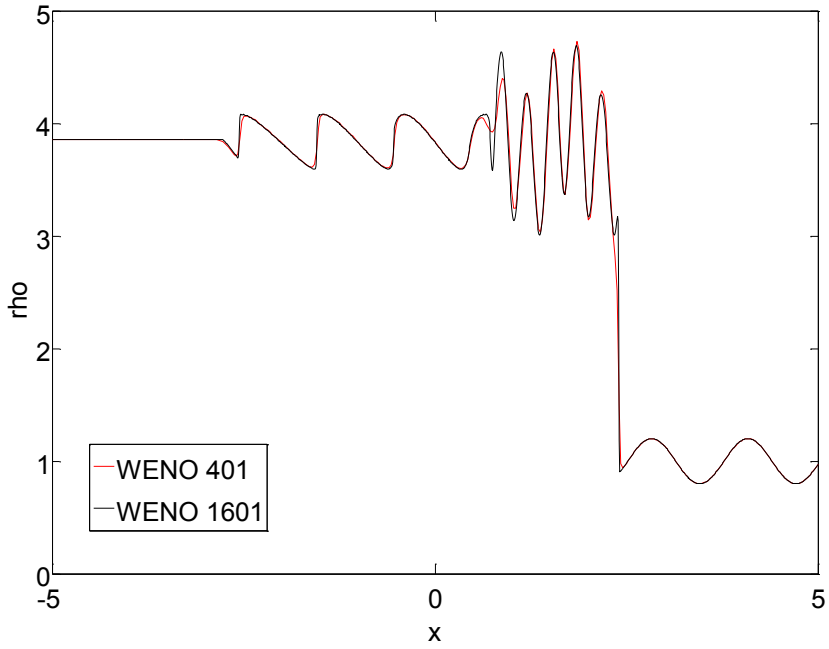

Figure 4-13 Density Solution of Shu-Osher Problem from WENO

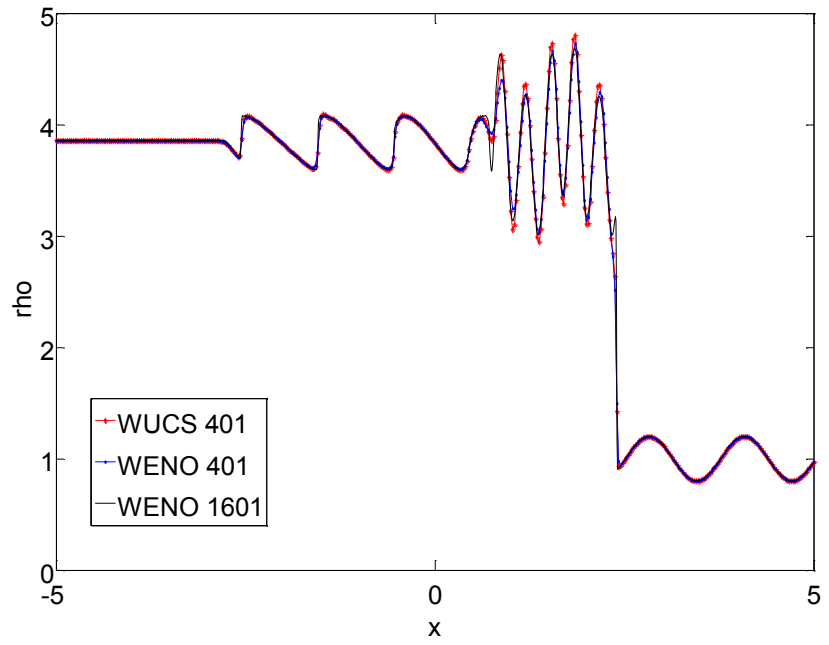

Figure 4-14 Enlargement of density solution of Shu-Osher problem

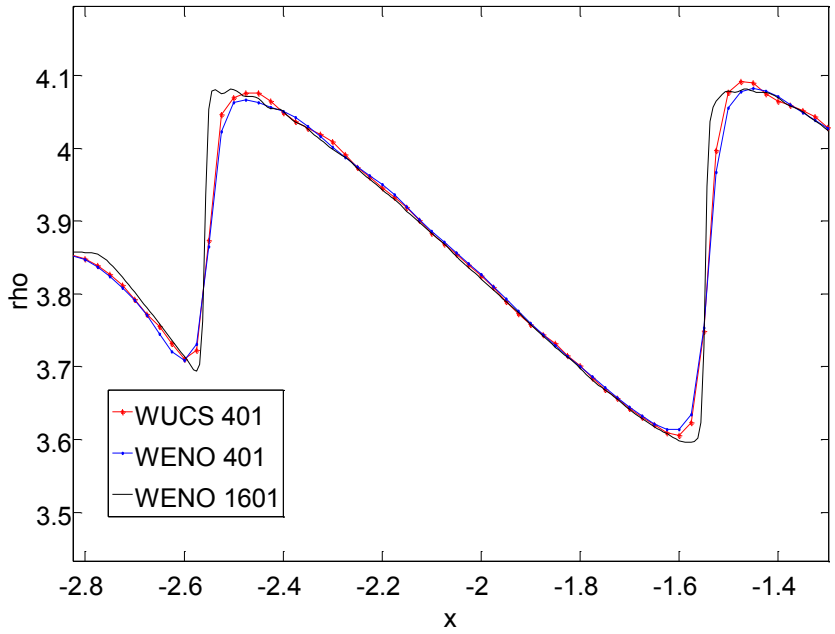

Figure 4-15 Enlargement of density solution of Shu-Osher problem

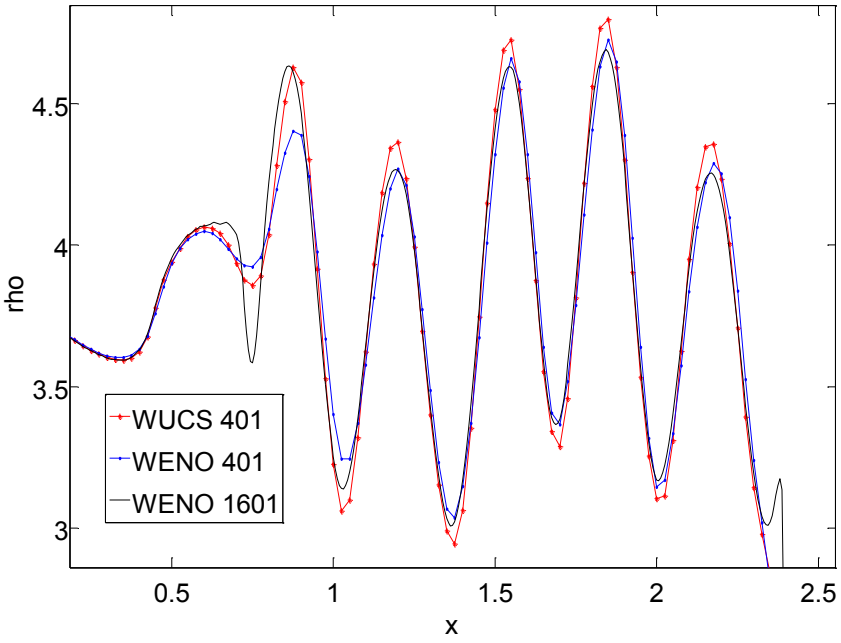

Figure 4-16 Enlargement of density solution of Shu-Osher problem

WUCS is capable of capturing the high frequencies waves generated in the upstream area of the shock. Figures 4-10, 4-11, 4-15 and 4-16 report detail enlargements of discontinuity areas in the upstream shock region, comparing the two different schemes. It can be observed that WUCS solution, compared to the fifth-order WENO solution, can capture the shock more sharply and has better resolution properties, and is free from numerical oscillations. In certain areas, the WUCS appears to be very close to the reference solution.

4.2.3 Two-Blast Wave

This one-dimensional test problem was introduced in [30] to illustrate the strong relationship between the accuracy of the overall flow solution and the thinness of discontinuities on the grid. It involves multiple interactions of strong shocks and rarefactions with each other and with contact discontinuities. This problem is extremely difficult to solve on a uniform Eulerian grid, although it poses no particular difficulty for a Lagrangian calculation. The initial condition consists of three constant states of a gamma-law gas, with γ = 1.4, which is at rest between reflecting walls separated by a distance of unity. The density is everywhere unity, while in the leftmost tenth of the volume the pressure is 1000, in the rightmost tenth it is 100, and in between it is 0.01. Two strong blast waves develop and collide, producing a new contact discontinuity. This evolution is quite complex [30]. The density solutions at t = 0.038 from both WUCS and WENO with same mesh of 201 points are shown in Figure 4-17. The reference density solution is from WENO with a finer mesh of 2401 points. Figure 4-18 is showing results from both schemes with same mesh of 401 points. It is very clear from Figure 4-17 and 4-18 that WUCS depict the density distribution more precisely with sharper shocks.

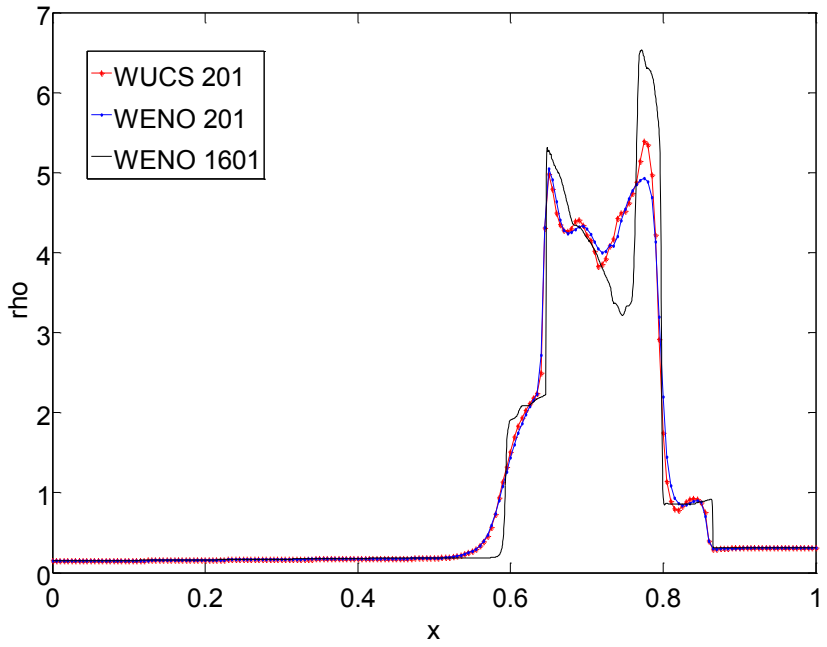

Figure 4-17 WUCS and WENO density solution of Two Blast Wave problem

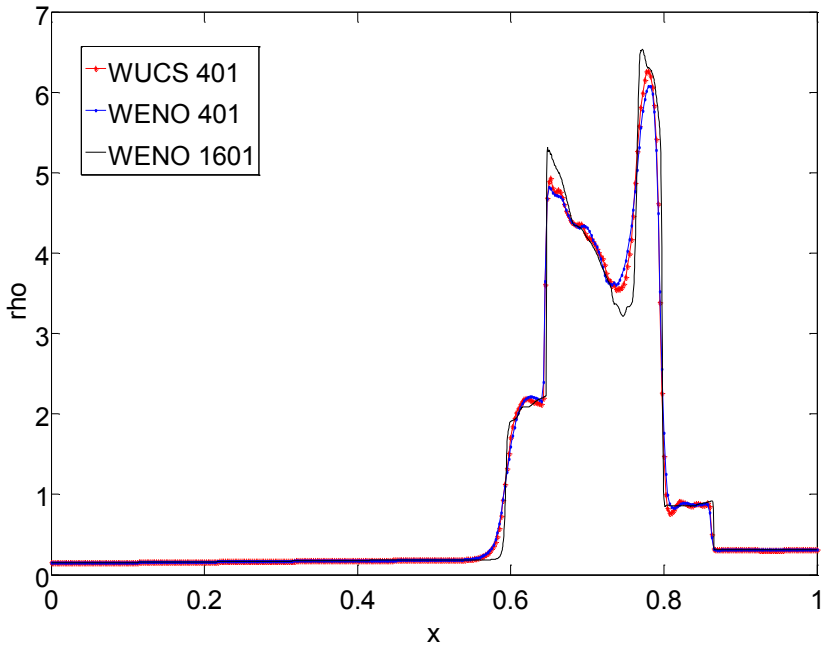

Figure 4-18 WUCS and WENO density solution of Two Blast Wave problem

4.3 Two-Dimensional Case

The two-dimensional Euler equations in vector and conservative form read as

$$\frac{\partial U}{\partial t}+\frac{\partial F}{\partial x}+\frac{\partial G}{\partial y}=0$$

$$U=(\rho,\rho u,\rho v,E_t)^T \tag{4.4}$$

$$F=(\rho u,\rho u^2+p,\rho uv,u(E_t+p))^T$$

$$G=(\rho v,\rho uv,\rho v^2+p,v(E_t+p))^T$$

In the following oblique shock reflection numerical case, $x \in (0,2)$, $y \in (0,1.1)$, and an uniform grid of 65×65 points is used. The Lax-Friedrichs flux-splitting is used, and the time quadrature is a fourth-order Runge-Kutta scheme. The test case is an oblique shock reflection on an inviscid wall which is showing as bottom in Figure 4-19, with shock angle of 35.24° and the mach number is 2. The boundary conditions at the top is inflow

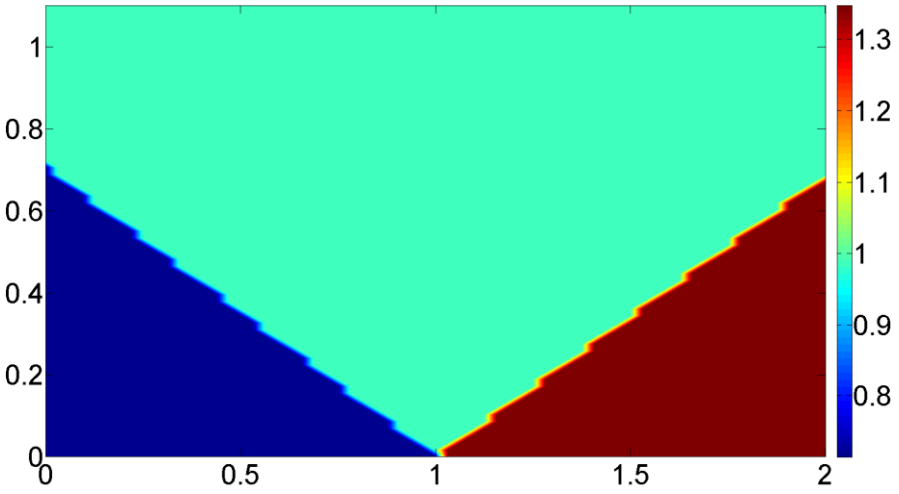

Figure 4-19 Analytic solution for pressure, 13 equally spaced contours

condition with $u=1.8618$, $v=-0.1957$, $\rho=1.2620$, $p=0.9908$. The left side boundary is also set as inflow conditions, but with $u=2$, $v=0$, $\rho=1$, $p=5/7$.

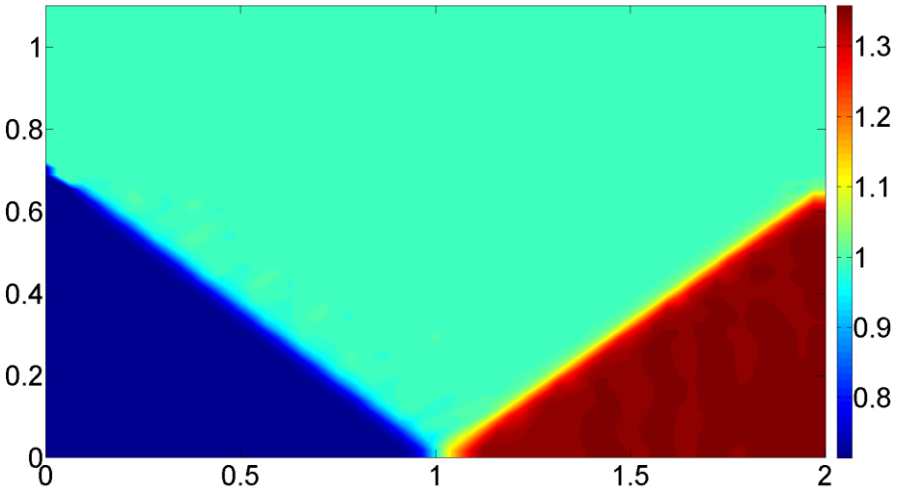

Figure 4-20 Pressure solution from WUCS

The right side boundary is set as outflow conditions calculated by extrapolation. Initial condition is that the oblique shock already hit the inviscid wall, but not reflects yet.

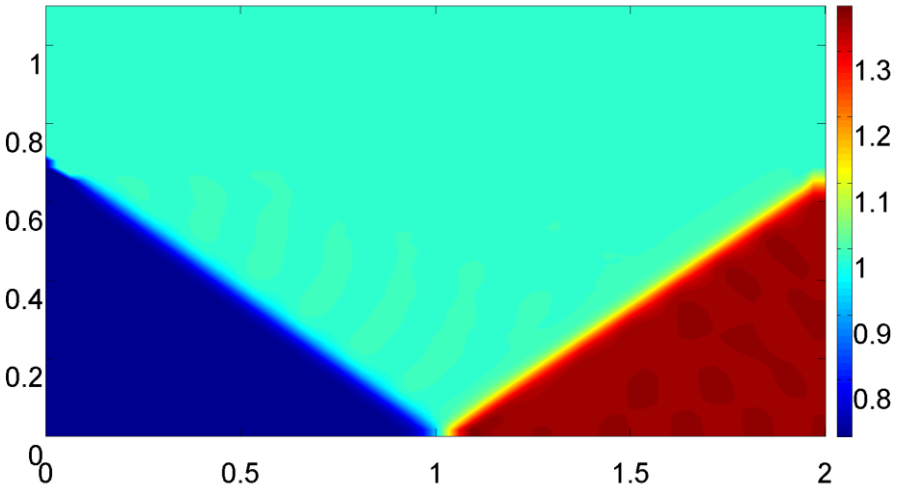

Figure 4-21 pressure solution from WENO

Figures 4-19, 4-20, 4-21 show the contour of the pressure p, from the analytical, WUCS and WENO solutions on 65×65 grids respectively. Figure 4-22, 4-23, 4-24 is the pressure comparison of analytical, WUCS and WENO solution at y = 11/64. Figure 4-25,

4-26, 4-27 is the density comparison of analytical, WUCS and WENO solution at y = 11/64. Comparing the two schemes, it is observed that the WUCS captures the shock more sharply than WENO scheme, and does not present larger numerical oscillations than WENO scheme.

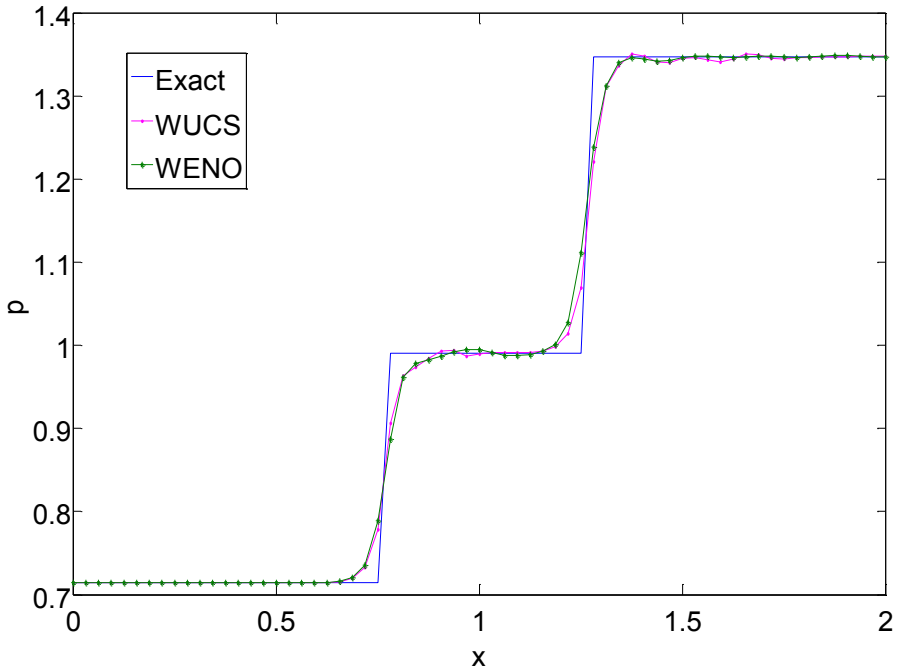

Figure 4-22 Pressure solution at y= 11/64

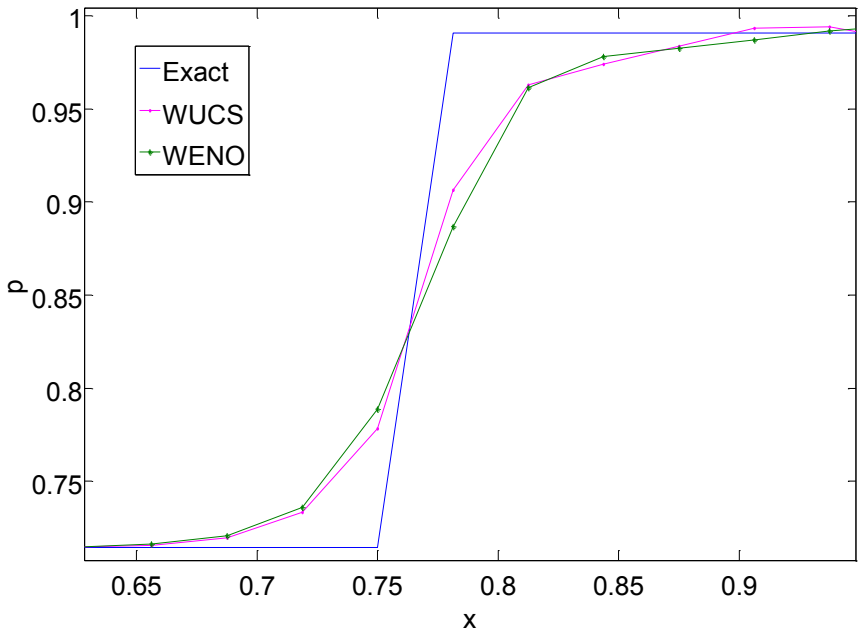

Figure 4-23 Enlargement of pressure solution at y= 11/64

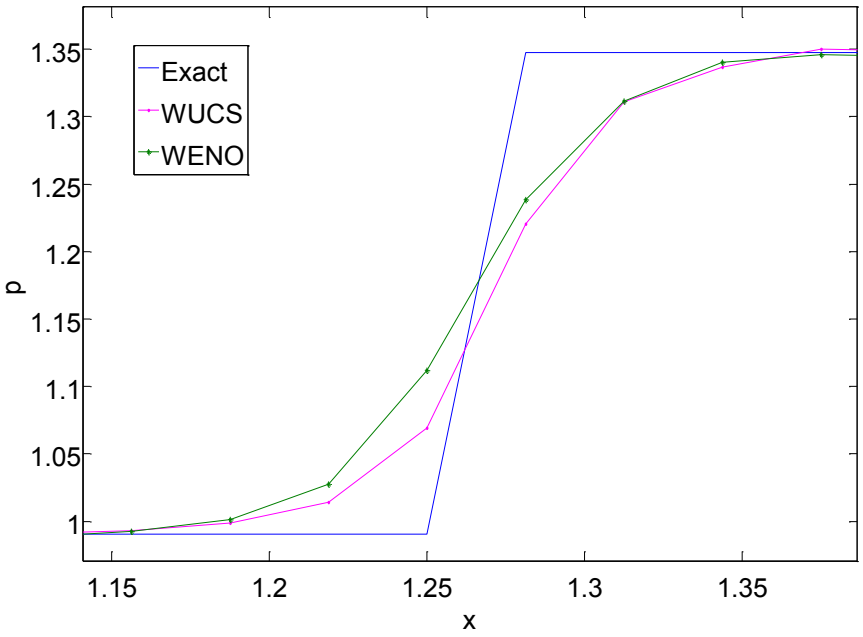

Figure 4-24 Enlargement of pressure solution at y= 11/64

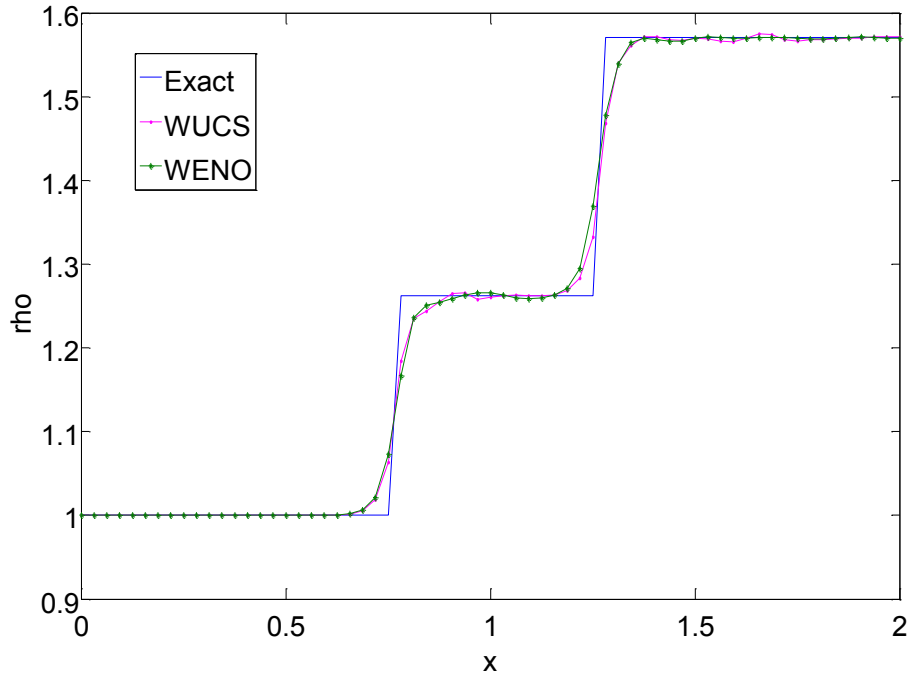

Figure 4-25 Density solution at y= 11/64

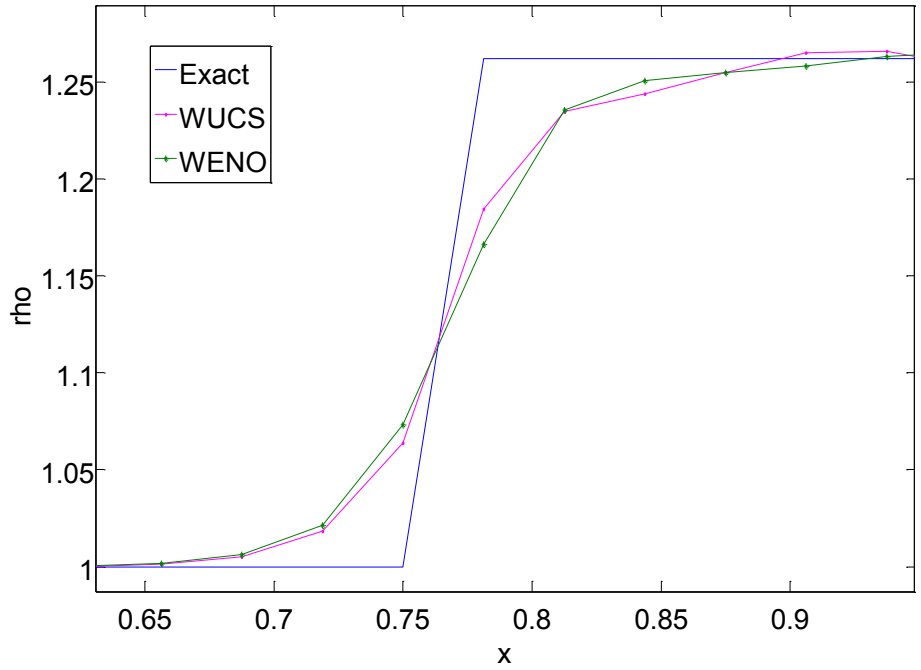

Figure 4-26 Enlargement of density solution at y= 11/64

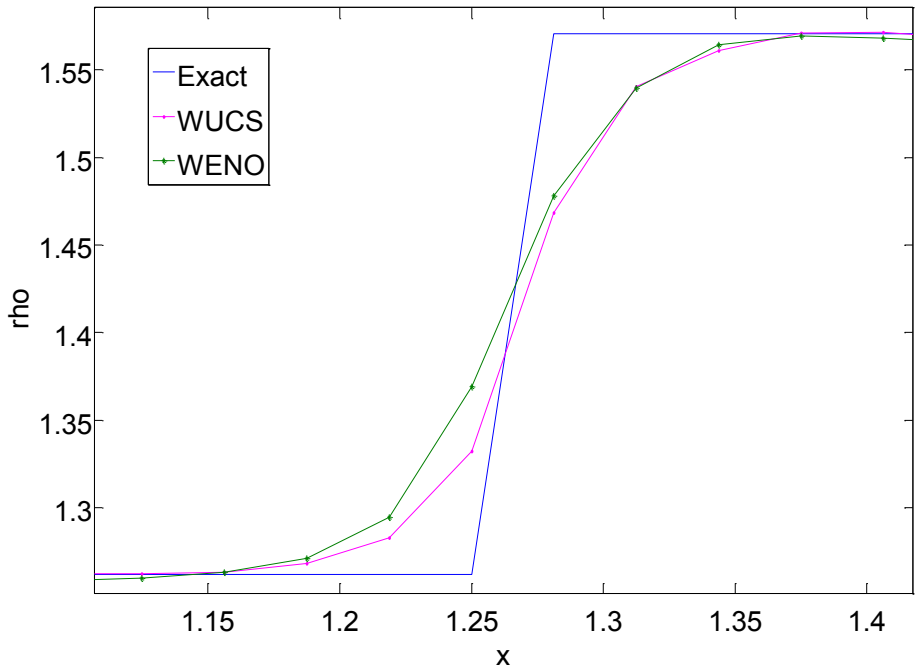

Figure 4-27 Enlargement of density solution at y= 11/64

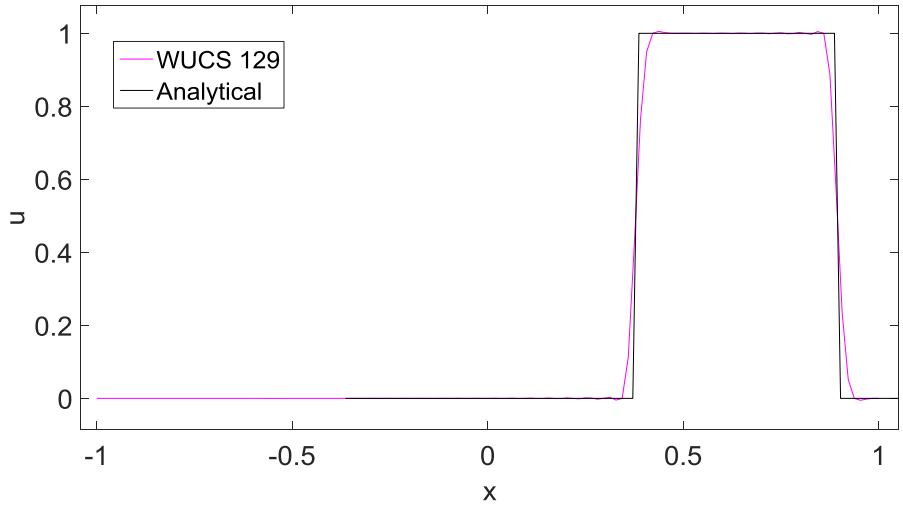

Figure 4-28 $u(t,x)$ with $t = 2/\pi$

4.4 Wave equation with jump initial condition

In this appedix, a simple numerical case is shown as an supplementation for WUCS. The numerical case is wave equation $\frac{\partial u}{\partial t}+\frac{\partial u}{\partial x}=0$

with initial condition $u(0,x)=\begin{cases}1 & -\frac{1}{4}\leq x\leq\frac{1}{4}\\ 0 & -1\leq x<-\frac{1}{4},\frac{1}{4}<x\leq 1\end{cases}$

The analytical solution is $u(t,x)=u(0,x-t)$

The numerical results from WUCS which is shown in Figure 4-28 clearly demonstrates that WUCS has strong capability to simulate discontinuities.

Chapter 5

New Method of Creating Global Weights for WUCS

Global Weights for WENO is firstly proposed in [33]. When applying the 5th Order WENO, for example, 2-Dimensional Euler equation problems, computing the weights of each stencil at each time step for each variable, which will cost fairly high CPU time. To save the CPU cost, computing the weights of some variables, for example, multiplication of velocity and pressure or multiplication of velocity and density, only once, and combine them to be the global weights before carrying out Runge–Kutta time marching method at each time step. Appreciably saving of CPU time can be found when applying this Global Weights in numerical scheme for particial differential equation solver.

An important technical issue for WUCS scheme is the selection of the weights for stencil candidates near the shock region. In fluid mechanics, the shock has large gradient in density and velocity. The pressure and energy discontinuity are synchronous with density and velocity. Therefore, the multiplication of density and velocity are important symbols or indication that can interpret rapid flow change. Meanwhile, density and velocity could have discontinuity in the contact surface according to the Riemann solution. Based on these understandings, choosing ρu, $u(E_t + p)$ to calculate global weights for 1D problem is a reasonable first try to step out for WUCS.

The test results showing below are using a computer which has a configuration of Intel® Core™ i3-2100 CPU, 16 GB RAM. In section 5.1 and 5.2, serial C codes have been used to the tests, and only one core in the CPU will be utilized in computation. In section 5.3, a parallel C code has been used, and four cores in the CPU are utilized. The difference between Global Weights WUCS and traditional weighted WUCS is only the way to calculate weights, and other parts of the codes are same.

5.1 SOD problem solved by WUCS with Global Weights

Same SOD problem as section 4.2.1 is used to test Global Weights WUCS. In Table 5-1, a comparison of wall time consumption by two ways for SOD problem is tabulated. About 6% wall time has been saved by Global Weights WUCS comparing with traditional weighted WUCS. Figure 5-1 shows the result of SOD problem using Global Weights WUCS. Comparing with Figure 4-2, a slightly larger over shooting has been noticed.

Table 5-1 Wall time comparison for SOD problem running

Grid Numbers	Global Weights	Traditional Weights
201	61.05 s	65.34 s
401	236.51 s	251.51 s

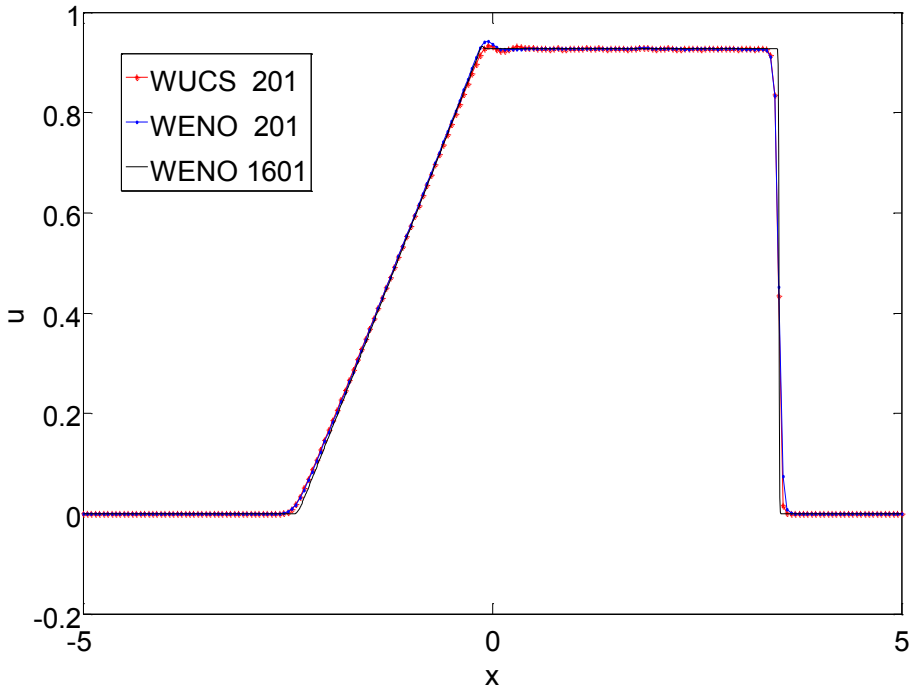

Figure 5-1 SOD problem velocity results from Global Weights WUCS

5.2 Shu-Osher problem solved by WUCS with Global Weights

Same Shu-Osher problem as section 4.2.2 is used to test Global Weights WUCS. In Table 5-2, a comparison of wall time consumption by two ways for Shu-Osher problem is tabulated. About 3~8% wall time has been saved by Global Weights WUCS comparing with traditional weighted WUCS. Figure 5-2 shows the result of Shu-Osher problem using Global Weights WUCS. Comparing with Figure 4-6, Global Weights WUCS got even better results.

Table 5-2 Wall time comparison for Shu-Osher problem running

Grid Numbers	Global Weights	Traditional Weights
201	53.22 s	58.14 s
401	460.95 s	476.85 s

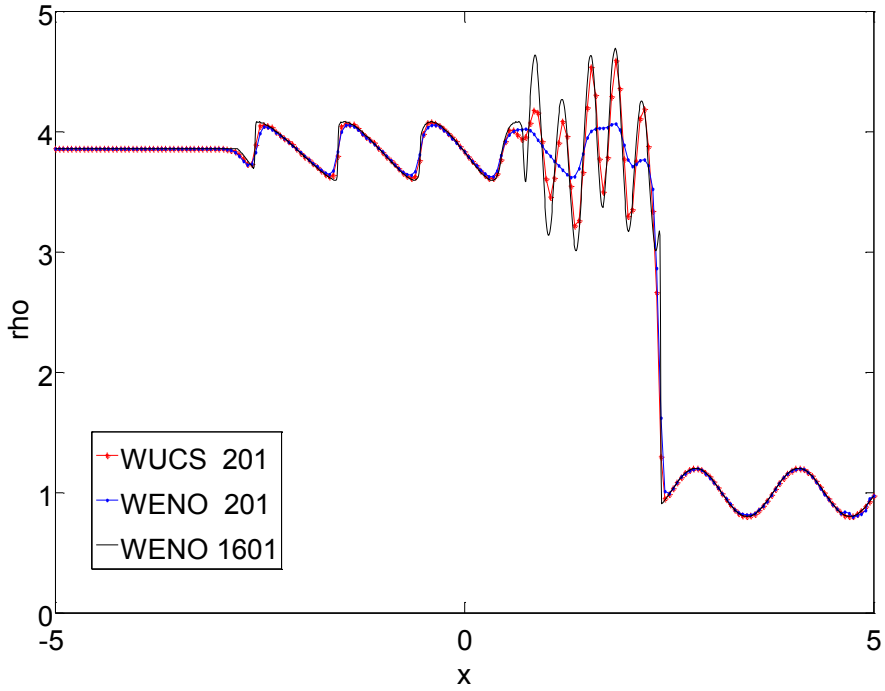

Figure 5-2 Shu-Osher problem results from Global Weights WUCS

5.3 Two Blast Wave problem solved by WUCS with Global Weights

Same Two Blast Wave problem as section 4.2.3 is used to test Global Weights WUCS. In Table 5-2, a comparison of wall time consumption by two ways for Two Blast Wave problem is tabulated. About 4.5% wall time has been saved by Global Weights WUCS comparing with traditional weighted WUCS. Figure 5-3 shows the result of Two Blast Wave problem using Global Weights WUCS. Comparing with Figure 4-15, Global Weights WUCS is showing similar results as calculated by traditional weighted WUCS.

Table 5-3 Wall time comparison for Two Blast Wave problem running

Grid Numbers	Global Weights	Traditional Weights
201	853.69 s	892.02 s
401	3181.49 s	3344.47 s

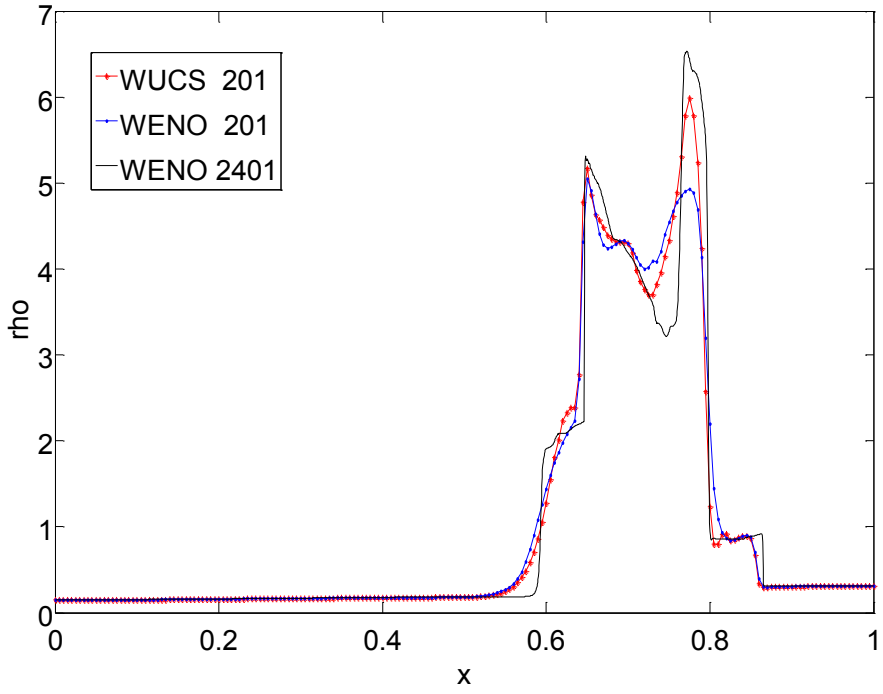

Figure 5-3 Two Blast Wave problem results from Global Weights WUCS

5.4 Summary of Global Weights WUCS

In this chapter, several numerical cases show that Global Weights WUCS has the feasibility and the capability to save CPU time without sacrificing accuracy and shock-capturing ability.

Chapter 6

Construction Methodology Application

In previous chapters, a construction methodology of weighted upwind compact scheme has been elaborated and justified. In this chapter, using the mentioned methodology with Legendre polynomial and different stencils, a new sixth order weighted upwind compact scheme (SWUCS) will be built and tested. This application will show the flexibility and potential capability of this methodology.

6.1 Legendre Polynomials

Legendre polynomials $P_n(x)$ with n = 0, 1, 2, …, are solutions to Legendre's ordinary differential equation:

$$\frac{d}{dx}[(1-x^2)\frac{d}{dx}P_n(x)] + n(n+1)P_n(x) = 0$$

They are both named after a French Mathematician, Adrien-Marie Legendre. Legendre ODE has regular singular points at $x = \pm 1$. Each Legendre polynomial $P_n(x)$ is an nth-degree polynomial. It may be expressed by Rodrigues' formula:

$$P_n(x) = \frac{1}{2^n n!}\frac{d^n}{dx^n}[(x^2-1)^n] \qquad n = 0, 1, 2, \ldots$$

The first few $P_n(x)$ are listed in Table 6-1.

Table 6-1 Legendre polynomials

n	$P_n(x)$
0	1
1	x
2	$\frac{1}{2}(3x^2-1)$
3	$\frac{1}{2}(5x^3-3x)$
4	$\frac{1}{8}(35x^4-30x^2+3)$
5	$\frac{1}{8}(63x^5-70x^3+15x)$
6	$\frac{1}{16}(231x^6-315x^4+105x^2-5)$

Table 6-1 -continued

7	$\frac{1}{16}(429x^7 - 693x^5 + 315x^3 - 35x)$

6.2 New Stencils for SWUCS

Similarly as section 2.3, for obtaining a 6th order weighted upwind compact scheme, three third-order approximations of the linear compact combination of numerical fluxes at $\hat{F}_{j-\frac{3}{2}}$, $\hat{F}_{j-\frac{1}{2}}$, $\hat{F}_{j+\frac{1}{2}}$, $\hat{F}_{j+\frac{3}{2}}$and $\hat{F}_{j+\frac{5}{2}}$ are obtained from the three candidate stencils (Fig. 2-1):

$$E^0_{SWUCS} = \{F_{j-2}, F_{j-1}, F_j\}$$

$$E^1_{SWUCS} = \{F_{j-1}, F_j, F_{j+1}\}$$

$$E^2_{SWUCS} = \{F_j, F_{j+1}, F_{j+2}\}$$

Choosing the Legendre polynomial for the third order approximation of $b_0\hat{F}_{j-\frac{3}{2}} + b_1\hat{F}_{j-\frac{1}{2}} + \hat{F}_{j+\frac{1}{2}}$, we obtain, for the first stencil E^0_{SWUCS}:

$$b_0\hat{F}_{j-\frac{3}{2}} + b_1\hat{F}_{j-\frac{1}{2}} + \hat{F}_{j+\frac{1}{2}} \approx (b_2F_{j-1} + b_3F_j)/h \tag{6.1}$$

$$b_1 = 2(1 + b_0)$$

$$b_2 = \frac{1}{2} + \frac{5b_0}{2}$$

$$b_3 = \frac{5}{2} + \frac{b_0}{2}$$

And similarly for the other two stencils E^1_{SWUCS} and E^2_{SWUCS}:

$$c_0\hat{F}_{j-\frac{1}{2}} + \hat{F}_{j+\frac{1}{2}} + c_1\hat{F}_{j+\frac{3}{2}} \approx (c_2F_j + c_3F_{j+1})/h \tag{6.2}$$

$$c_1 = \frac{1}{2} - c_0$$

$$c_2 = \frac{1}{4} + 2c_0$$

$$c_3 = \frac{5}{4} - 2c_0$$

$$\hat{F}_{j+\frac{1}{2}} + d_0\hat{F}_{j+\frac{3}{2}} + d_2\hat{F}_{j+\frac{5}{2}} \approx (d_2F_{j+1} + d_3F_{j+2})/h \tag{6.3}$$

$$d_1 = \frac{1}{2}(-2 + d_0)$$

$$d_2 = 2 + \frac{d_0}{4}$$

$$d_3 = -2 + \frac{5d_0}{4}$$

For obtaining 6th order of $C^0_{SWUCS}E^0_{SWUCS} + C^1_{SWUCS}E^1_{SWUCS} + C^2_{SWUCS}E^2_{SWUCS}$, b_0, c_0, d_0, C^0_{SWUCS}, C^1_{SWUCS}, and C^2_{SWUCS} need satisfy

$$b_0 = -\frac{-92C^0_{SWUCS} + 7C^1_{SWUCS} - 20C^2_{SWUCS}}{168C^0_{SWUCS}}$$

$$c_0 = -\frac{-8C^0_{SWUCS} - 7C^1_{SWUCS} + 8C^2_{SWUCS}}{28C^0_{SWUCS}} \tag{6.4}$$

$$d_0 = -\frac{-20C^0_{SWUCS} + 7C^1_{SWUCS} - 260C^2_{SWUCS}}{84C^0_{SWUCS}}$$

Like WENO, this 6th weighted upwind compact scheme will use non-linear weights ω^i_{SWUCS} instead C^i_{SWUCS}

$$\omega^{i,j\pm\frac{1}{2}}_{SWUCS} = \frac{\gamma^{i,j\pm\frac{1}{2}}_{SWUCS}}{\sum_{k=0}^{2}\gamma^{k,j\pm\frac{1}{2}}_{SWUCS}} \qquad \gamma^{i,j\pm\frac{1}{2}}_{SWUCS} = \frac{C^i_{SWUCS}}{(\varepsilon + IS_{i,j\pm\frac{1}{2}})^p} \qquad i = 0,1,2 \tag{6.5}$$

And $\omega^0_{SWUCS}E^0_{SWUCS} + \omega^1_{SWUCS}E^1_{SWUCS} + \omega^2_{SWUCS}E^2_{SWUCS}$ is defined as 6th weighted upwind compact scheme (SWUCS).

6.3 Dissipation and Dispersion of SWUCS

6.3.1 Left Stencil

E^0_{SWUCS} is represented by (6.1). This section E^0_{SWUCS} 's dissipation and dispersion are listed below.

$$w'_r = \frac{(8(1 + b_0 + {b_0}^2) + (1 + b_0(10 + b_0))\mathrm{Cos}(w))\mathrm{Sin}(w)}{5 + b_0(8 + 5b_0) + 4(1 + b_0)^2\mathrm{Cos}(w) + 2b_0\mathrm{Cos}(2w)}$$

$$w'_i = \frac{4(-1+{b_0}^2)\mathrm{Sin}(\frac{w}{2})^4}{5+b_0(8+5b_0)+4(1+b_0)^2\mathrm{Cos}(w)+2b_0\mathrm{Cos}(2w)}$$

By similar method initiated in section 2.6.1, a simple dissipation error condition is setup as

$$\left.\frac{4(-1+{b_0}^2)\mathrm{Sin}(\frac{w}{2})^4}{5+b_0(8+5b_0)+4(1+b_0)^2\mathrm{Cos}(w)+2b_0\mathrm{Cos}(2w)}\right|_{w=\pi} > 0$$

That is,

$$b_0 < -1 \text{ or } b_0 > 1 \tag{6.6}$$

6.3.2 Center Stencil

E^1_{SWUCS} is represented by (6.2). This section E^1_{SWUCS}'s dissipation and dispersion are listed below.

$$w'_r = \frac{(-8(1-2c_0+4{c_0}^2)+(-1+16c_0(-1+2c_0))\mathrm{Cos}(w))\mathrm{Sin}(w)}{-5+4c_0-8{c_0}^2-4\mathrm{Cos}(w)+4c_0(-1+2c_0)\mathrm{Cos}(2w)}$$

$$w'_i = \frac{4(1-4c_0)\mathrm{Sin}(\frac{w}{2})^4}{-5+4c_0-8{c_0}^2-4\mathrm{Cos}(w)+4c_0(-1+2c_0)\mathrm{Cos}(2w)}$$

A simple dissipation error condition is setup as

$$\left.\frac{4(1-4c_0)\mathrm{Sin}(\frac{w}{2})^4}{-5+4c_0-8{c_0}^2-4\mathrm{Cos}(w)+4c_0(-1+2c_0)\mathrm{Cos}(2w)}\right|_{w=\pi} > \frac{1}{10}$$

That is,

$$c_0 > 1/4 \tag{6.7}$$

6.3.3 Combine Methodology Application

Since upwind scheme will only use left stencil and/or center stencil around shock, only (6.6) and (6.7) will be combined with (6.4) for SWUCS coefficients calculation. The results of combination of (6.4), (6.6), and (6.7) is

$C^0_{SWUCS} > C^2_{SWUCS}$ and $C^1_{SWUCS} > (260C^0_{SWUCS} + 20C^2_{SWUCS})/7$

$C^0_{SWUCS} = 1.2$, $C^1_{SWUCS} = 60$, and $C^2_{SWUCS} = 1$ have been selected from above range. Then by (6.4), $b_0 = -181/126 \;\; c_0 = 527/2100 \;\; d_0 = -34/21$

6.4 Numerical Test

Order test results for SWUCS is tabulated in Table 6-2 and Table 6-3. It can show that SWUCS has expected 6th order accuracy as section 6.2. In the following order test, p is chosen as 5, and ε is chosen to be 10^{-5} in accordance with (6.5).

6.4.1 SWUCS order test by Sin(πx)

$$f(x) = \mathrm{Sin}(\pi x) \qquad -1 \le x \le 1$$
$$f'(x) = \pi \mathrm{Cos}(\pi x) \qquad -1 \le x \le 1$$

Table 6-2 Errors of the numerical derivative of Sin(πx)

Grid Points	Error Infinity-Norm	Error Order	Error Two-Norm	Error Order
9	6.79E-01		9.22E-01	
17	4.21E-02	4.01	5.05E-02	4.19
33	6.07E-04	6.12	6.88E-04	6.20
65	5.51E-07	10.10	9.64E-07	9.48
129	8.01E-09	6.10	1.39E-08	6.12
257	7.25E-11	6.79	3.05E-10	5.51
513	9.27E-13	6.29	8.24E-12	5.21

6.4.2 SWUCS order test by $\mathrm{Sin}^2(\pi x)$

$$f(x) = \mathrm{Sin}^2(\pi x) \qquad -1 \le x \le 1$$
$$f'(x) = \pi \mathrm{Sin}(2\pi x) \qquad -1 \le x \le 1$$

Table 6-3 Errors of the numerical derivative of $\mathrm{Sin}^2(\pi x)$

Grid Points	Error Infinity-Norm	Error Order	Error Two-Norm	Error Order
9	1.02E+01		1.08E+01	
17	4.69E-01	4.44	6.19E-01	4.13
33	1.31E-03	8.48	3.23E-03	7.58

Table 6-3 -continued

65	2.20E-05	5.90	4.70E-05	6.10
129	3.66E-07	5.91	8.47E-07	5.79
257	4.05E-09	6.50	1.42E-08	5.90
513	4.03E-11	6.65	3.14E-10	5.50

6.4.3 Sod Shock-Tube

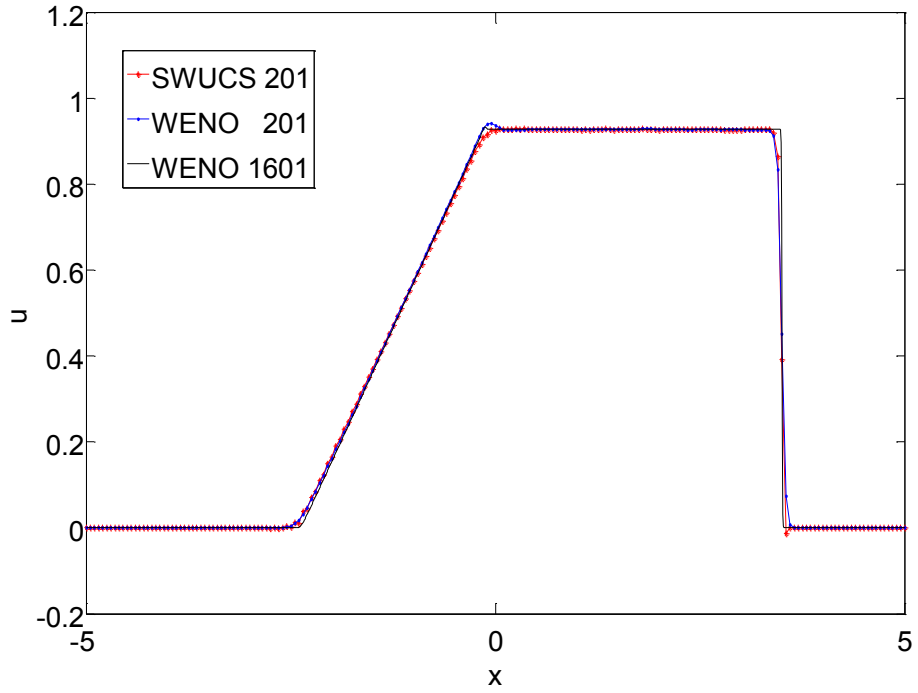

Figure 6-1 Velocity Solution from SWUCS for SOD

Use the same SOD shock-tube problem as section 4.2.1 to test this SWUCS. The velocity results with a mesh of 201 points is shown in Figure 6-1. Some oscillation has been notice before after shock. A tiny overshooting can be found around shock in downstream side. Overall, SWUCS is giving a fine results.

6.4.4 Shu-Osher Problem

Use the same Shu-Osher problem as section 4.2.2 to test this SWUCS. The density results is shown in Figure 6-2. SWUCS is showing a fairly nice results.

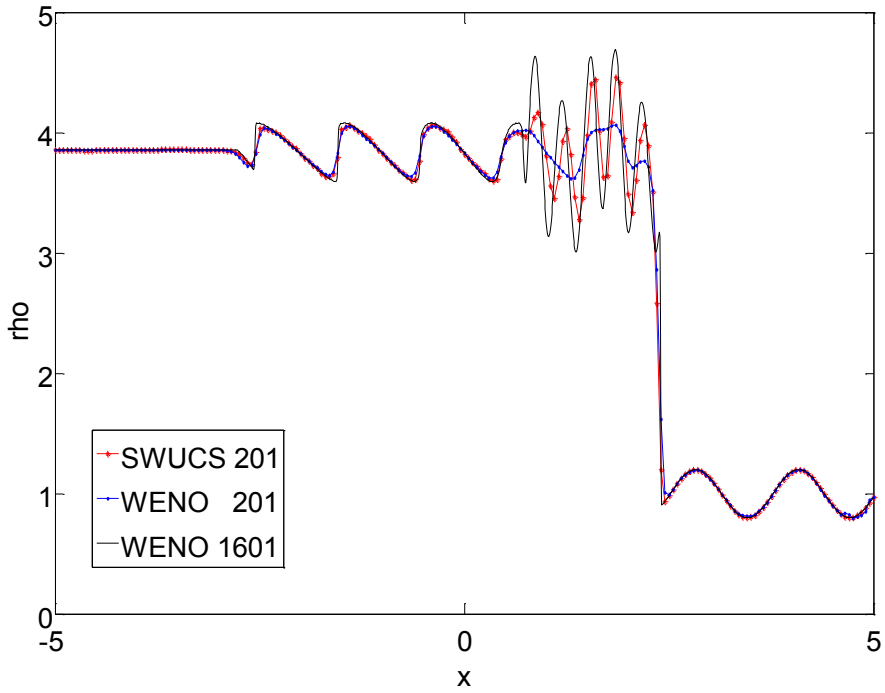

Figure 6-2 Density Solution from SWUCS for Shu-Osher problem

Chapter 7

Conclusion and Discussion

A construction methodology of weighted upwind compact scheme has been initially elaborated from dissipation and dispersion perspective. Two different schemes have been setup. And several CFD cases have been used to testify these two schemes and the construction methodology.

The construction methodology can derive a parameter weighted upwind compact scheme not only has high order accuracy in smooth area or for smooth function, but also the capability of shock-capturing. WUCS is the first scheme derived by this construction methodology. WUCS has expected seventh order accuracy in smooth area, also with flexibility and strong capability of shock-capturing. SWUCS is another simplified application of this construction methodology. SWUCS expands this construction methodology into Legendre polynomials and a different stencil structure. This expansion can prove that this construction methodology has flexibility for more different applications.

The most difficult and sensitive step is to choose a better dissipation error and dispersion error condition for left stencil and right stencil. If a large or loose dissipation error and dispersion error condition is chosen, the combined inequalities will have a large range which is hard to fix the parameters. If choosing by the other way, the combined inequalities will has no solution which means no parameter can be found for expected accuracy and shock-capturing abilities.

Future work may be extended to dissipation and dispersion nonlinear system optimization, or possibly quantitatively designated dissipation and dispersion for each stencil and also for the combined scheme.

References

[1] Tim Colonius, Sanjiva K. Lele, “Computational aeroacoustics: progress on nonlinear problems of sound generation”. Progress in Aerospace Sciences, Volume 40, Pages 345–416, 2004

[2] Mike Bahorich, Steve Farmer, “3-D seismic discontinuity for faults and stratigraphic features: The coherence cube”. The Leading Edge, Volume 14, Pages 1053-1058, October 1995

[3] Rama Cont, Ekaterina Voltchkova, “A Finite Difference Scheme for Option Pricing in Jump Diffusion and Exponential Levy Models”. SIAM Journal on Numerical Analysis, Volume 43, No. 4, Pages 1596 – 1626

[4] Peter Lynch, “The Emergence of Numerical Weather Prediction: Richardson's Dream”, Cambridge University Press, ISBN 978052185729, November 2006

[5] Bram van Leer, “CFD Education: Past, Present, Future”, AIAA 99-0910, A99-16738

[6] R. Courant, K. Friedrichs, H. Lewy, “On the Partial Difference Equations of Mathematical Physics”. Mathematische Annalen, Volume 100, Issue 1, Pages 32-74, 1928

[7] Rainer Ansorge, Thomas Sonar, “Mathematical Models of Fluid Dynamics: Modelling, Theory, Basic Numerical Facts - An Introduction, 2nd, Updated Edition”, Wiley, ISBN: 978-3-527-40774-3, August 2009

[8] J. VonNeumann, R. D. Richtmyer, “A Method for the Numerical Calculation of Hydrodynamic Shocks”. Journal of Applied Physics, Volume 21, Pages 232; doi: 10.1063/1.1699639, 1950

[9] Richard Courant, Eugene Isaacson, Mina Rees, “On the solution of nonlinear hyperbolic differential equations by finite differences”, Communications on Pure and Applied Mathematics, Volume 5, Issue 3, Pages 243–255, August 1952

[10] Jaw-Yen Yang, “Second- and Third-order Upwind Difference Schemes for Hyperbolic Conservation Laws”. NASA, NASA Technical Memorandum 85959 July 1984.

[11] Peter D. Lax, “Weak solutions of nonlinear hyperbolic equations and their numerical computation”. Communications on Pure and Applied Mathematics, Volume 7, Issue 1, Pages 159–193, February 1954

[12] K. O. Friedrichs, “Symmetric hyperbolic linear differential equations”. Communications on Pure and Applied Mathematics, Volume 7, Issue 2, Pages 345–392, May 1954

[13] Alexander Kurganov, Eitan Tadmor, “New High-Resolution Central Schemes for Nonlinear Conservation Laws and Convection–Diffusion Equations”. Journal of Computational Physics, Volume 160, Pages 241–282, 2000

[14] Godunov S K, “A difference method for the numerical calculation of discontinuous solutions of hydrodynamic equations”. Matematicheskii Sbornik, Volume 47, Pages 271-306, 1959

[15] P. D. Lax, “Hyperbolic systems of conservation laws II”. Communications on Pure and Applied Mathematics, Volume 10, Issue 4, Pages 537–566, February 1957

[16] Peter Lax, Burton Wendroff, “Systems of Conservation Laws”. Communications on Pure and Applied Mathematics, Volume 13, Issue 2, Pages 217–237, February 1960

[17] Yan Chao, Yu Jian, Xu Jinglei, Fan Jingjing, Gao Ruize, Jiang Zhenhua, “On the Achievements and Prospects for the Methods of Computational Fluid Dynamics”. Advances in Mechanics, Volume 41, No. 5, Sep. 25, 2011

[18] Robert MacCormack, “The Effect of Viscosity in Hypervelocity Impact Cratering”. Journal of Spacecraft and Rockets, Volume 40, No. 5, Pages 757-763, 2003

[19] R. W. MacCormack, “A Numerical Method for Solving the Equations of Compressible Viscous Flow". AIAA Journal, Volume 20, No. 9, Pages 1275-1281, 1982

[20] Bkam Van Leer, “Towards the Ultimate Conservative Difference Scheme”. V. A Second-Order Sequel to Godunov’s Method”. Journal of Computational Physics, Volume 32, Pages 101-136, 1979

[21] MUSCL scheme, http://en.wikipedia.org/wiki/MUSCL_scheme

[22] Ami Harten, “High Resolution Schemes for Hyperbolic Conservation Laws”. Journal of Computational Physics, Volume 49, Pages 357-393, 1983

[23] Ami Harten, Bjorn Engquist, Stanley Osher, Sukumar R. Chakravarthy, “Uniformly High Order Accurate Essentially Non-oscillatory Schemes, III”. Journal of Computational Physics, Volume 71, Pages 231-303, 1987

[24] Xu-Dong Liu, Stanley Osher, Tony Chan, “Weighted Essentially Non-oscillatory Schems”. Journal of Computational Physics, Volume 115, Pages 200-212, 1994

[25] Sanjiva K. Lele, “Compact Finite Difference Schemes with Spectral-like Resolution”. Journal of Computational Physics, Volume 103, Pages 16-42, 1992

[26] Maria Luisa Bambozzi Oliveira, “High-order numerical schemes for high-speed flows”, PhD dissertation. Mathematics dept., University of Texas at Arlington, August 2009

[27] G.S. Jiang and C.W. Shu, “Efficient implementation of weighted ENO scheme”. Journal of Computational Physics, Volume 126, Pages 202-228, 1996

[28] Robert Vichnevetsky, John B. Bowles, “Fourier Analysis of Numerical Approximations of Hyperbolic Equations”. SIAM, Philadelphia, 1982

[29] N. N. Mansour, P. Moin, W. C. Reynolds, and J. H. Ferziger, “Turbulent Shear Flows I”. Springer-Verlag, New York/Berlin, Pages 386, 1977

[30] Paul Woodward, “The Numerical Simulation of Two-Dimensional Fluid Flow with Strong Shocks”. Journal of Computational Physics, Volume 54, Pages 115-173, 1984

[31] Chi-Wang Shu, Stanley Osher, “Efficient implementation of essentially non-oscillatory shock-capturing schemes”. Journal of Computational Physics, Volume 77, Issue 2, Pages 439–471, August 1988

[32] Gary A Sod, “A survey of several finite difference methods for systems of nonlinear hyperbolic conservation laws”. Journal of Computational Physics, Volume 27, Issue 1, Pages 1–31, April 1978

[33] Huankun Fu, Zhengjie Wang, Yonghua Yan, Chaoqun Liu, “Modified weighted compact scheme with global weights for shock capturing”. Computers and Fluids, Volume 96, Pages 165–176, 13 June 2014

Biographical Information

Zhengjie Wang has received a Bachelor of Engineering degree in Ship Design and Marine Engineering, and a Master of Science degree in Mathematics. His research at the University of Texas at Arlington includes CFD, Large Eddy Simulation, and Numerical Scheme. His engineering experience includes optimized hull design, optimized mooring system design, and floating units' onboard software development.